ABSTRACT

Experiments in thin sheets of mercury and water have shown that the dynamics of bubble rise are similar in aqueous and liquid metal systems.

An experimental investigation into the removal of hydrogen from molten steel into low flow rate jets of argon has shown that hydrogen concentrations of less than 2 ppm are readily attainable.

Argon efficiencies in the order of 80% of theoretical were obtained.

Calculations based upon argon bubbling for hydrogen removal and low flow rate argon jetting for surface protection suggest that the argon jet will consume only a few percent of total argon utilized to ensure a final hydrogen concentration of less than 2 ppm in steel.

HYDROGEN REMOVAL FROM STEEL

BY

MARIO PANENI

A Thesis Presented for the Masters Degree
in Metallurgical Engineering

Department of Metallurgical Engineering
McGill University
Montreal
August, 1969

TABLE OF CONTENTS

PART I

TABLE OF CONTENTS (Cont'd)

PART II

TABLE OF CONTENTS (Cont'd)

1.0 THE INVESTIGATION

This study was designed to examine two aspects of hydrogen elimination from molten steel.

1. Rate and dynamic behaviour of bubbles in liquid metals.
2. Rates of hydrogen elimination from steel using a low velocity jet degassing technique.

The investigation of bubble behaviour arises from the development of the inert gas flushing technique in which bubbles are introduced at the bottom of a bath of molten steel and from the likelihood that in vacuum degassing, hydrogen effuses into rising bubbles of CO produced by the reaction of carbon and oxygen in steel.

The second part of the work, jet degassing of steel, was examined for the case of low velocity jets. This work was prompted by the facts that:

(a) Degassing by inert gas bubbling uses inert gas efficiently but the minimum hydrogen content (≈ 3 ppm) is not satisfactory.

(b) High velocity jet degassing reduces the hydrogen content sufficiently but the gas efficiency is less than 1/10 of theoretical.

Low velocity jetting in conjunction with inert bubbling might be satisfactory on both grounds.

1.1 REMOVAL OF HYDROGEN FROM STEEL

The presence of hydrogen in steel may result in defects in steel products.

Two types of defects are (i) blowholes and (ii) flaking of the steel surface. Both defects arise when molten steel, high in dissolved hydrogen, solidifies more quickly than the hydrogen can effuse from the metal.

Hydrogen is considerably less soluble in solid steel than in molten steel (Figure 1.1-1) and as a result the solid steel is supersaturated in hydrogen.

It is generally considered that during hot working hydrogen effuses from the metal into any voids or discontinuities in the steel. These gas filled voids cannot be eliminated from the solid steel and always remain as defects in the steel.

If the gas filled pores are near the metal surface the high hydrogen pressure in the pores may result in the breaking of the surface in the form of blowholes and flakes.

The content of hydrogen in molten steel is rarely greater than 10 ppm. The source of hydrogen is water vapour in the air or water in the scrap charge.

Industrial steelmaking operations have shown that the harmful effects of hydrogen are eliminated if the hydrogen contents are below 2 ppm.

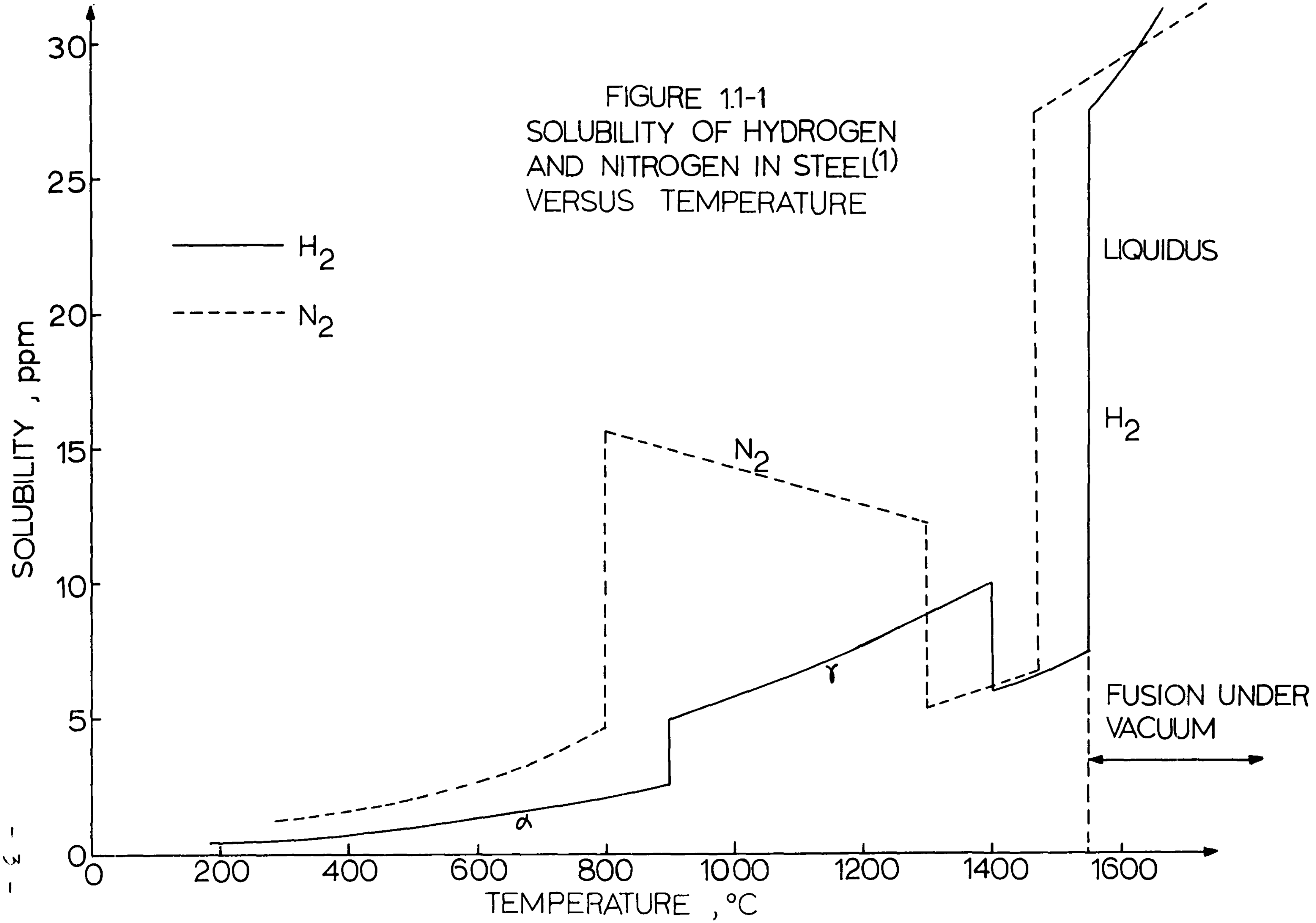

FIGURE 1.1-1
SOLUBILITY OF HYDROGEN AND NITROGEN IN STEEL(1) VERSUS TEMPERATURE

1.2 COMMERCIAL DEGASSING TECHNIQUES

The most prominent techniques for the degassing of steel are:

1. Ladle degassing.
2. Vacuum stream degassing.
3. Pipette degassing.
4. Continuous degassing by siphon method.
5. Inert gas flushing (submerged nozzle).
6. Jet degassing.

The operation of these degassing techniques is described in Table 1.2-1.

Each of these techniques has been studied from the point of view of determining the degree to which hydrogen can be removed and, with the exception of inert flush degassing, each has been shown to be able to reduce hydrogen levels of below 2 ppm.

Table 1.2-1

Types of degassing techniques and method of degassing(2)

Ladle degassing	Vacuum stream degassing	Pipette degassing
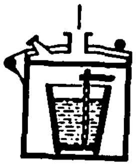 A	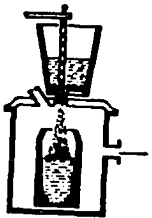	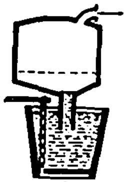 C
Molten steel is poured into the treatment ladle held inside the vacuum tank. The pressure is reduced to 2-10 mm Hg and the metal is held under vacuum for 5-10 minutes.	Steel is held in a ladle sealed on top of the vacuum tank. When the stopper is opened the metal melts through an aluminum rupture disc and is spray cast into an ingot mould or ladle held inside the vacuum tank. In vacuum the metal stream breaks into droplets which subdivide as they fall, thereby exposing a large surface area of metal to vacuum. Pressure 0.3-1 mm Hg.	The metal is drawn into a vacuum tank repetitively by raising and lowering either the ladle or the tank. Pressure 1-10 mm Hg.

Table 1.2-1 (Cont'd)

Continuous degassing by siphon method	Inert gas flushing	Vacuum stream degassing
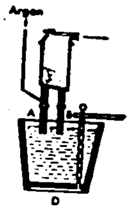 A tank is suspended above the ladle containing the molten steel. Two legs dip into the molten steel and the tank pressure is reduced to 1-2 mm Hg. The metal rises in both legs and an inert gas is introduced into one leg, reducing the bulk density of steel which sprays upward inside the vacuum tank and is degassed. The metal returns to the ladle via the other leg.	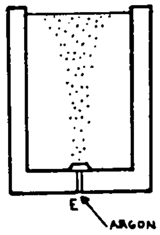 Argon gas is blown into the molten steel via a porous plug, submerged lance, or tuyere.	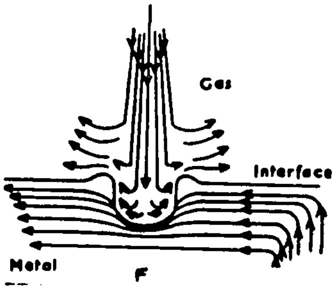 Argon gas is blown onto the surface of molten steel via one or more lances. .

PART I

LOW TEMPERATURE WORK: BUBBLE DYNAMICS

2.0 PREVIOUS WORK: ROOM TEMPERATURE INVESTIGATION

A Shapes and Velocities of Bubbles in Clear Liquids

Shapes and velocities of bubbles rising in clear liquids have been extensively studied.(3-12) Bubble behaviour can be categorized into three types of behaviour in order of increasing volume.

(i) Spherical bubbles, linear rise. Surface tension forces predominate at these small volumes. Rising velocities are similar to velocities predicted by Stokes' Law i.e.,

$$U = \frac{2}{9} \frac{g\, r_e^2}{\mu} (\rho_L - \rho_g)^* \quad \text{Eq. 2.0-1}$$

(ii) Ellipsoidal Bubbles, helical rise. Rising velocities are less than those predicted by Stokes' Law.

(iii) Spherical cap bubbles (spherical upper surface, planar under surface), linear rise. Fluid dynamic forces predominate at these large volumes.

The volume range over which each of these behaviour types occurs is dependent upon the properties of the fluid.

Haberman and Morton(5) have made a comprehensive review of the literature and report that in liquids for which the dimensionless parameter is

$$\frac{g\,\mu_L^4}{\rho_L\,\gamma^3} \qquad \text{(MORTON NUMBER)}$$

greater than 10^{-4} the ellipsoidal type of behaviour is not observed.

---

* A list of symbols appears on page 87

Hartunian and Sears(6) have studied the transition region between spherical and ellipsoidal forms. They report that for all systems in which the Reynolds Number,

$$\frac{2 r_e U \rho_L}{\mu_L} \qquad \text{(REYNOLDS NUMBER)}$$

is less than 200, the bubbles are spherical.

Above Reynolds Numbers of 200 the form of the bubbles is predicted by the magnitude of the Weber Number,

$$U (\rho_L r_e/\gamma)^{1/2} \qquad \text{(WEBER NUMBER)}$$

ellipsoidal bubbles being invariably observed (where Morton Number $< 10^{-4}$) above Weber Number values of 1.25.

Haberman and Morton(5) report that bubbles are spherical cap shaped in all liquids when the Weber Number exceeds 3.

Observed velocities of bubbles in liquids are shown in Figure 2.0-1.

B Velocities of Bubbles Rising in Liquid Metals

Davenport, Bradshaw and Richardson(7) have studied the velocities of bubbles rising in mercury and in molten silver. Guthrie(8) has investigated velocities of bubbles in molten silver.

These workers report (Figures 2.0-2, 2.0-3) velocities very similar to those reported for water in similarly sized columns of liquid.

C Shapes of Bubbles Rising in Liquid Metals

The only reported investigation into shapes of bubbles rising in molten metals is that of Davenport et al.(9) who used an

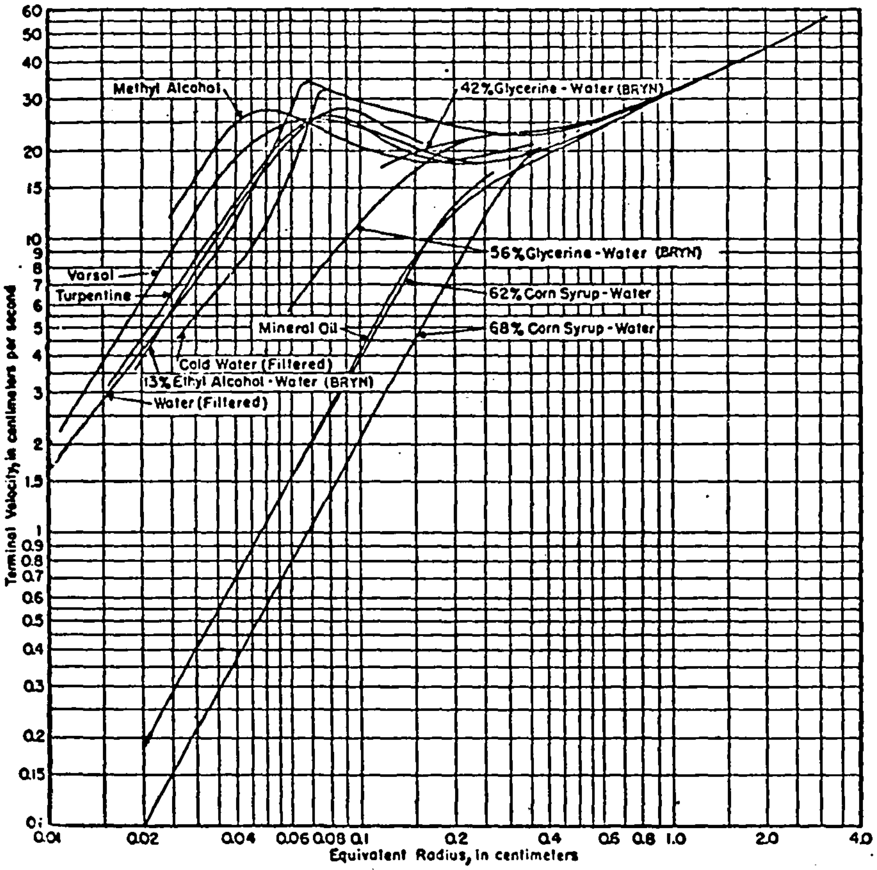

—COMPARISON OF TERMINAL VELOCITIES OF AIR BUBBLES IN VARIOUS LIQUIDS

Figure 2.0-1 Velocities of Bubbles Rising in Various Liquids(5)

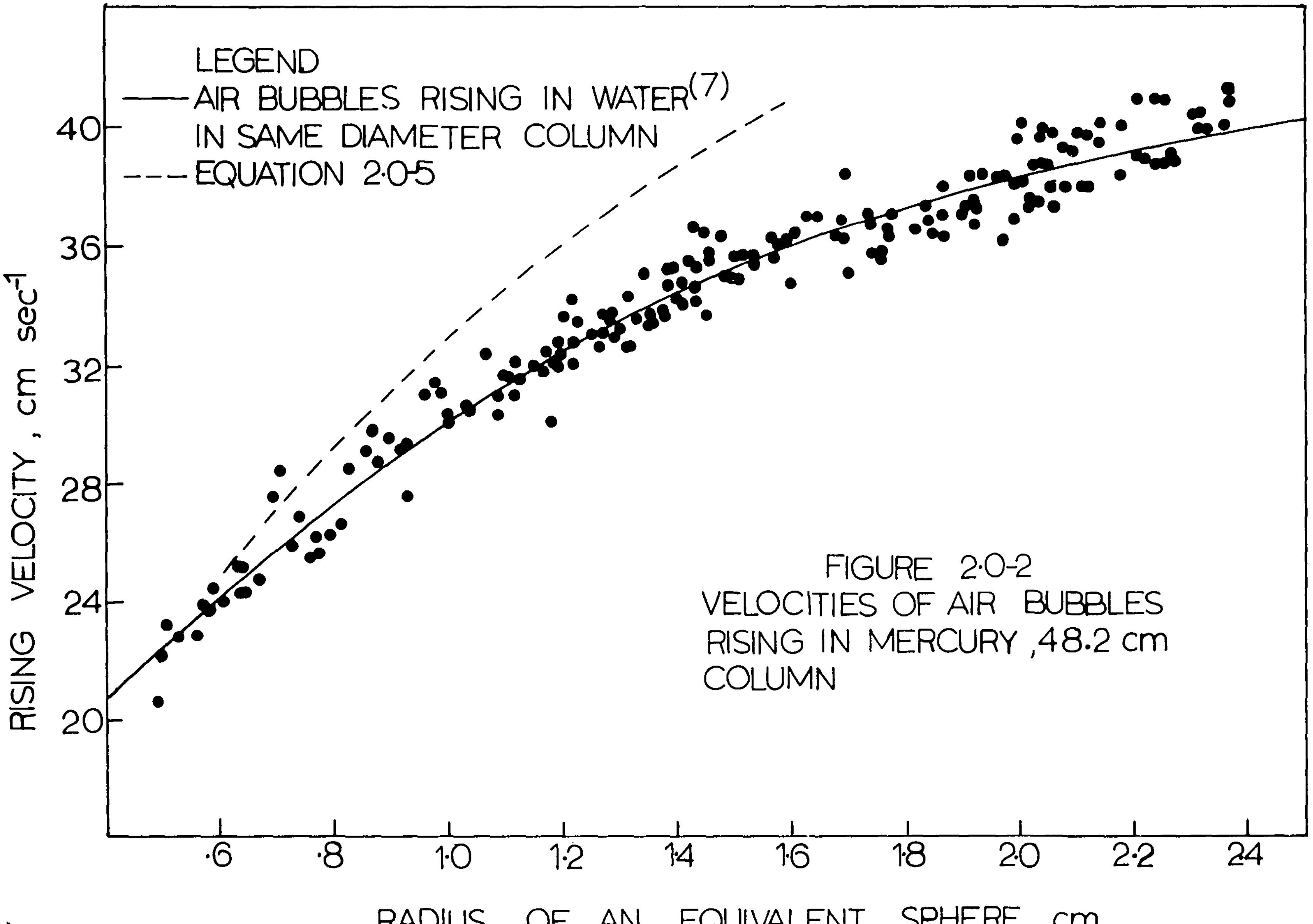

FIGURE 2·0·2
VELOCITIES OF AIR BUBBLES RISING IN MERCURY, 48·2 cm COLUMN

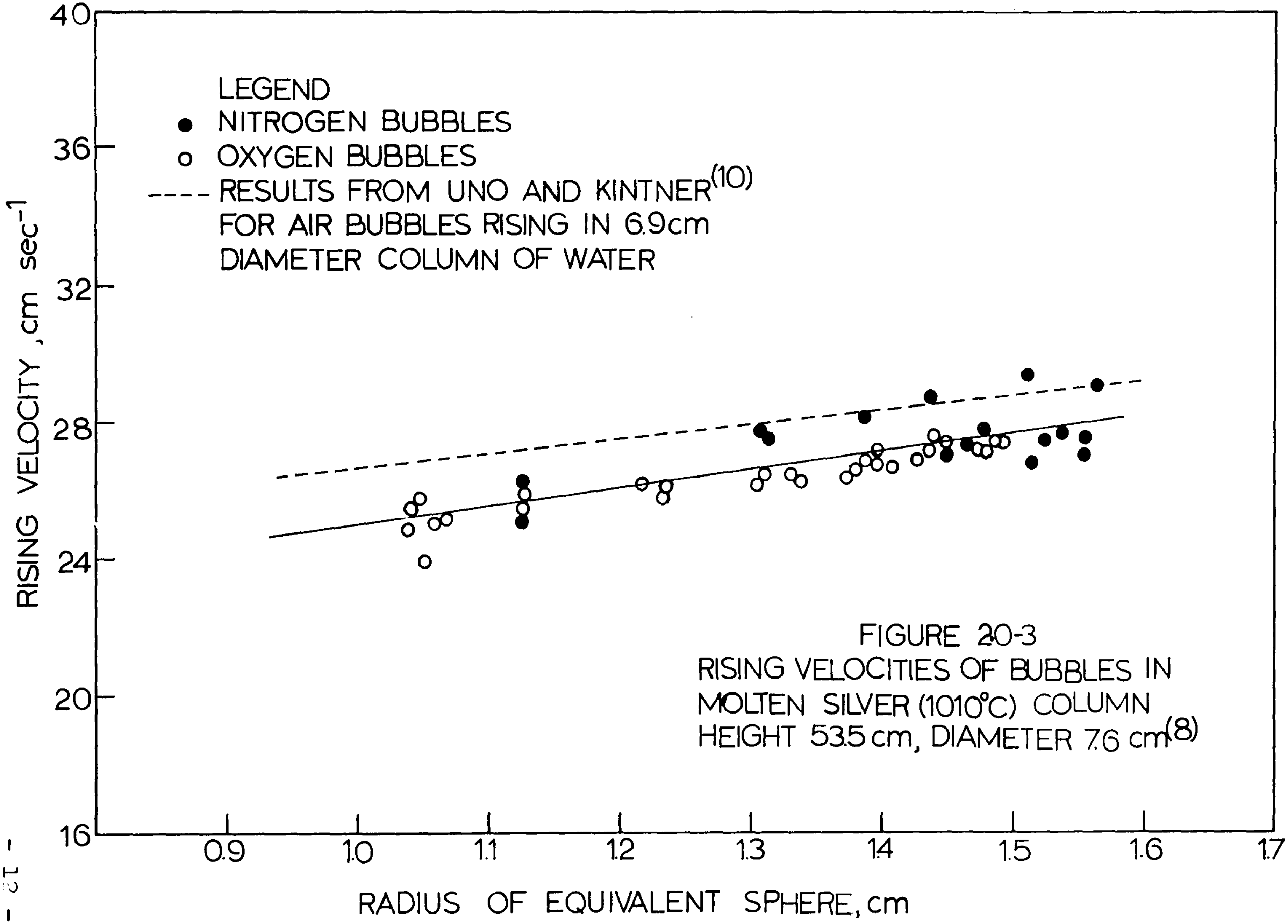

FIGURE 20-3
RISING VELOCITIES OF BUBBLES IN MOLTEN SILVER (1010°C) COLUMN HEIGHT 53.5 cm, DIAMETER 7.6 cm(8)

electric probe technique to determine

(a) the shape of the maximum planar area.

(b) the height near the vertical axis of the bubble.

They report (Figure 2.0-4) heights of bubbles similar to heights observed in water and basal radii some 10-15% smaller than in water.

These authors suggest that the smaller basal radii are due to the higher surface tension forces in the mercury, i.e.,

$$\gamma_{Hg} = 487 \text{ dynes cm}^{-1}, \qquad \gamma_{H_2O} = 72.8 \text{ dynes cm}^{-1}$$

which may cause the trailing edges of the bubbles to be rounded.

D Velocities of Spherical Cap Bubbles

Davies and Taylor(11) showed that application of the Bernoulli equation to flow around a spherical surface of constant total pressure leads to the relationship:

$$q^2 = 2\,gx = 2gR_c\,(1-\cos\theta) \qquad \text{Eq. 2.0-2}$$

These authors developed an expression for rising velocity by combining equation 2.0-2 with the expression for irrotational flow around a spherical surface:

$$q^2 = 9/4\;U^2 \sin^2\theta \qquad \text{Eq. 2.0-3}$$

The resulting expression:

$$U^2 = 8/9\;gR_c\;\frac{(1-\cos\theta)}{(\sin^2\theta)} \qquad \text{Eq. 2.0-4}$$

was applied to the forward stagnation point ($\theta = 0$) from which:

$$U = 2/3\;(gR_c)^{1/2} \qquad \text{Eq. 2.0-5}$$

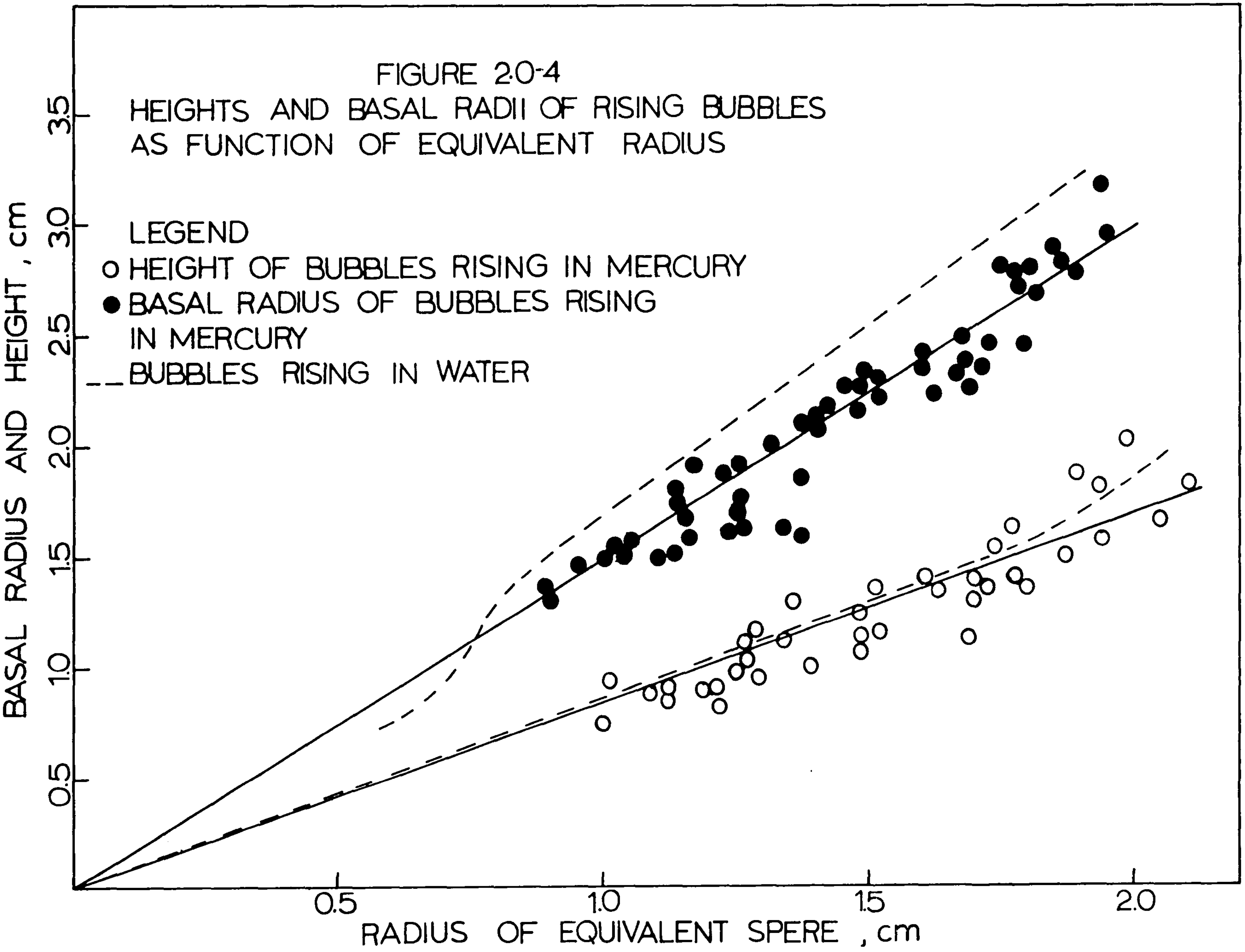

FIGURE 2.0-4

HEIGHTS AND BASAL RADII OF RISING BUBBLES AS FUNCTION OF EQUIVALENT RADIUS

Equation 2.0-5 gives excellent agreement with actual velocities in aqueous systems.

Equation 2.0-5 also indicates that the properties of the liquid should have no effect on rising velocity.

More recent experiments in viscous liquids have shown(9) that although Equation 2.0-5 holds, the shape of the bubble alters so that for a given volume of bubble, velocities are slightly lower in viscous liquids.

E Theoretical Models: Rising Velocity and Shape

The Davies and Taylor model is empirical in the sense that it makes no prediction as the angle which will be subtended by the forward cap surface, i.e., velocity and shape are not predicted as a function of volume.

Recently Davidson and Rippin(12) presented a model which assumes potential flow around the cap surface and the existance of an infinite stagnant wake. The model predicts a subtended angle, α, of 50° (see Figure 2.3-1, page 39) in reasonable agreement with experiment.

The Davidson and Rippin model predicts, however, velocities some 30% higher than experimental velocities.

F Velocities in Sheets of Liquid

Collins(13) applied the Davies and Taylor interpretation to the case of a bubble rising in a thin sheet of liquid. He showed that in the case of irrotational flow around a cylindrical front surface the surface velocity is

$$q^2 = 4 U^2 \sin^2 \theta \qquad \text{Eq. 2.0-6}$$

Combination of Equation 2.0-2 and Equation 2.0-6 at the forward stagnation point ($\theta = 0$) leads to the rising velocity expression:

$$U = \tfrac{1}{2} (g R_c)^{1/2} \qquad \text{Eq. 2.0-7}$$

2.1 EXPERIMENTAL EQUIPMENT AND PROCEDURE: ROOM TEMPERATURE INVESTIGATION

The room temperature investigation was undertaken to determine the dynamic behaviour of single bubbles rising in mercury and in water.

The experiments were carried out using a thin sheet of liquid in which bubbles rising in mercury could be visually observed. Thus, the thin liquid sheet experiments provided a means by which the behaviour of bubbles rising in water and in liquid metal (mercury) could be compared.

In each liquid the shapes and rising velocities of single bubbles rising in a thin (0.47 cm) sheet of liquid were obtained using both single frame and cine photography. Bubble volumes ranged from 0.4 cm^3 to 7.0 cm^3 in mercury, and from 0.2 cm^3 to 3.0 cm^3 in water.

A Apparatus

Shapes and velocities of bubbles were examined in a perspex container 80 cm high and 30 cm wide. The thickness of the space for the liquid sheet was 0.47 cm (Figure 2.1-1, A & B). Bubbles were formed by means of a rotating cup mechanism consisting of a hemispherical stainless steel inverted cup (Figure 2.1-2).

Nitrogen was introduced through the axle of the cup. Single bubbles were created by rotating the cup into the upright position.

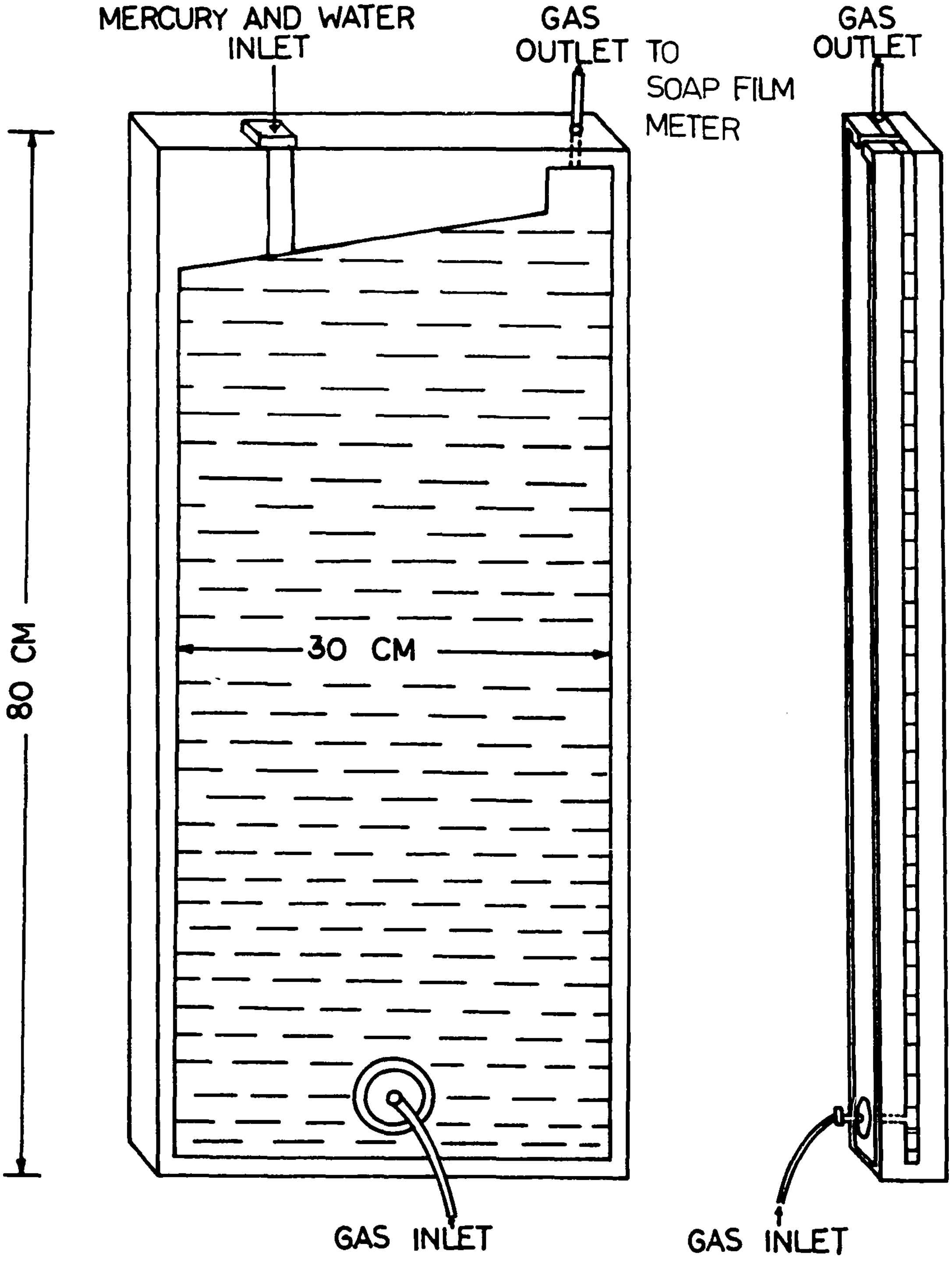

FIG. A FIG. B

FIGURE 2.1-1 PERSPEX CONTAINER DIAGRAM

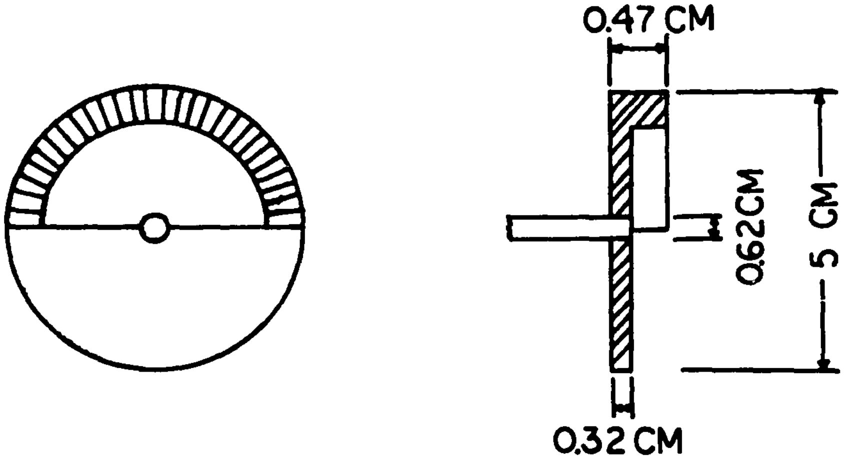

FIGURE 2.1-2
CUP DETAILS DIAGRAM

B Materials

Mercury:	Technical Grade purified mercury (98.9 - 99% Hg) purified by Johnson Matthey and Mallory, 110 Industry Street, Toronto 15, Ontario.
Water:	Distilled water.
Nitrogen:	Technical Grade purified nitrogen (Canadian Liquid Air), 99.99% N_2, 0.01% O_2, Trace Argon.

C Measurement of Bubble Volume

Bubble volumes were measured by means of the displacement technique developed by Baird and Davidson.(14)

A gas space was left between the liquid surface and the gas-tight perspex lid to which a soap film meter was connected. Movement of the soap film provided a direct measurement of bubble volume.

D Photographic Determination of Shapes and Rising Velocities

Shapes and velocities of rising bubbles were determined by photographic methods. Shapes were examined using a single frame camera and an electronic flash while velocities were examined using a cine camera. The photographs were taken with the bubble not less than 20 cm above the cup in order to minimize the effect of cup rotation on the mode of rise.

(i) Techniques

Single frame photographs (Film: Kodak Verichrome Pan V P 127) of bubble shapes were taken using a 4 cm x 4 cm

Rolleiflex camera (Rolleiflex-Rolleicord, Franke and Heidecke; Braunschweig, West Germany; Rolleinard No. 3 close-up lens) placed 20 cm from the apparatus. The aperture of the camera varied from f_{11} to f_{22} depending on the position of the flash unit. The flash unit (Metz 502 Mecablitz, Metz, Berlin; flash period 1/1000 sec.) placement varied between 30 cm and 100 cm from the apparatus.

The dimensions of the rising bubbles were determined directly by attaching a transparent ruler to the apparatus.

Bubble velocities were determined using an H 16 Bolex Reflex 16 mm movie camera (Paillard S.A. Saint Croix, Switzerland) at 64 frames per second, using Eastman Kodak Tri X reversal film. Lighting was provided by two 500 watt photoflood lamps set 30 cm out on each side of the front face of the apparatus. An Omega stopwatch with a precision of 1/100 second was set on the apparatus within the photographic field to determine the rising time of each bubble.

(ii) Interpretation of film

The photographs taken with the Rolleiflex were enlarged 12 times and the dimensions of bubbles were determined by comparison with the centimeter rule. Linear dimensions could be interpreted to ± 0.1 cm. Errors were due in part to the ripples that appeared on the bubble surfaces and to some light reflection. Depth of field errors were not encountered as the liquid sheet was only 0.47 cm thick.

Rising distance and time were determined by reference to the rule and to the stopwatch in each frame. Time and distance uncertainties of ± .02 seconds and ± 0.1 cm give rise to velocity uncertainties in the order of ± 5%.

2.2 EXPERIMENTAL RESULTS: ROOM TEMPERATURE

A Shapes of Rising Bubbles

Photographs of bubbles rising in water and in mercury are shown in Figures 2.2-1, 2.2-2 and 2.2-3.

At the larger sizes the typical cap shape of bubbles rising in three dimensional liquids is shown. Smaller bubbles are cylindrical or in the form of an elliptical cylinder.

Quantitative evaluations of shapes are tabulated in tables 2.2-1 and 2.2-2 for various heights of liquid above the cap.

Maximum horizontal (w) and vertical (h) dimensions, and volumes of bubbles (V), (as determined by displacement measurements) are tabulated.

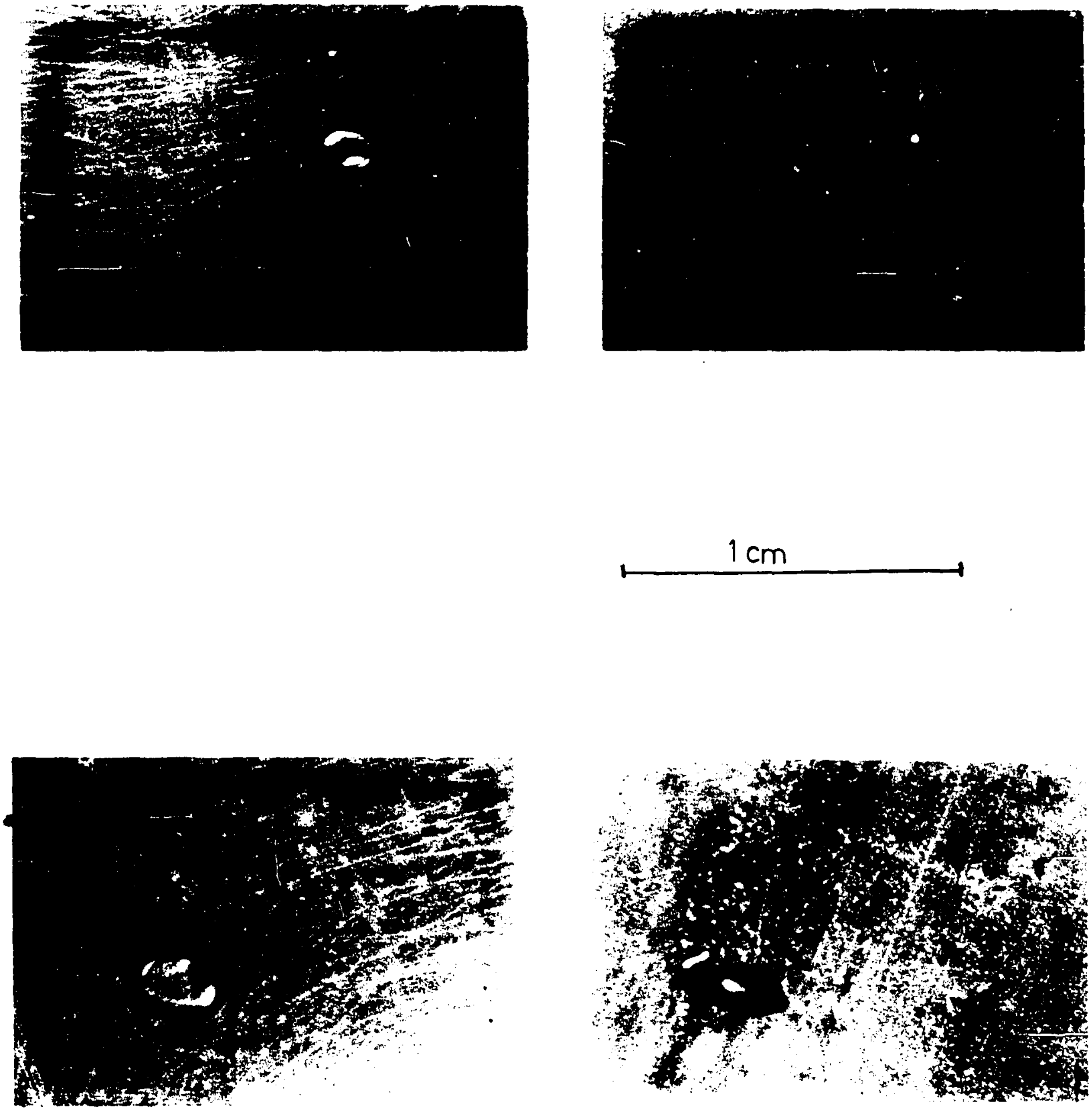

Figure 2.2-1 Bubbles Rising in Water (left) and in Mercury (right).

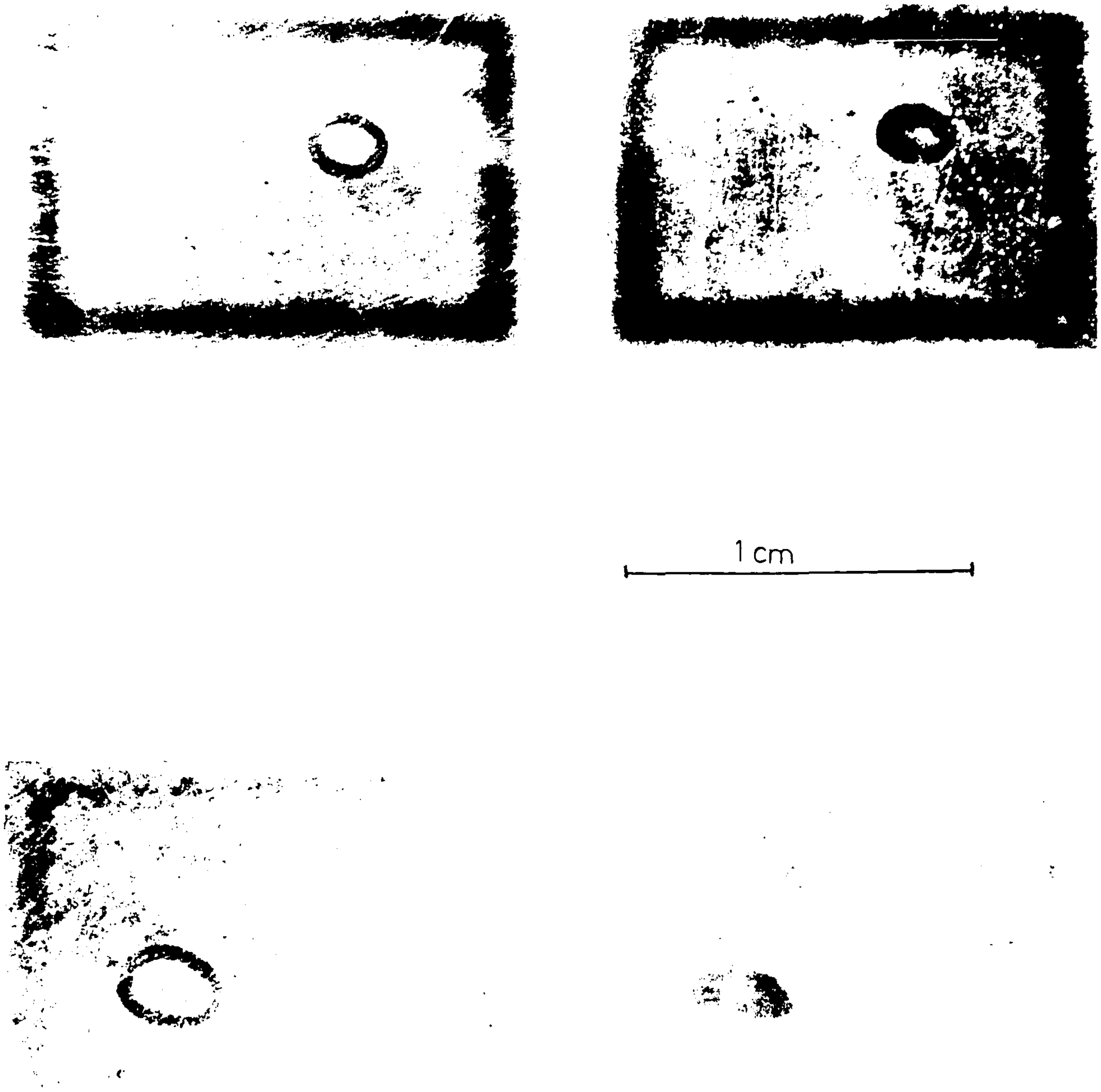

Figure 2.2-1 Bubbles Rising in Water (left) and in Mercury (right).

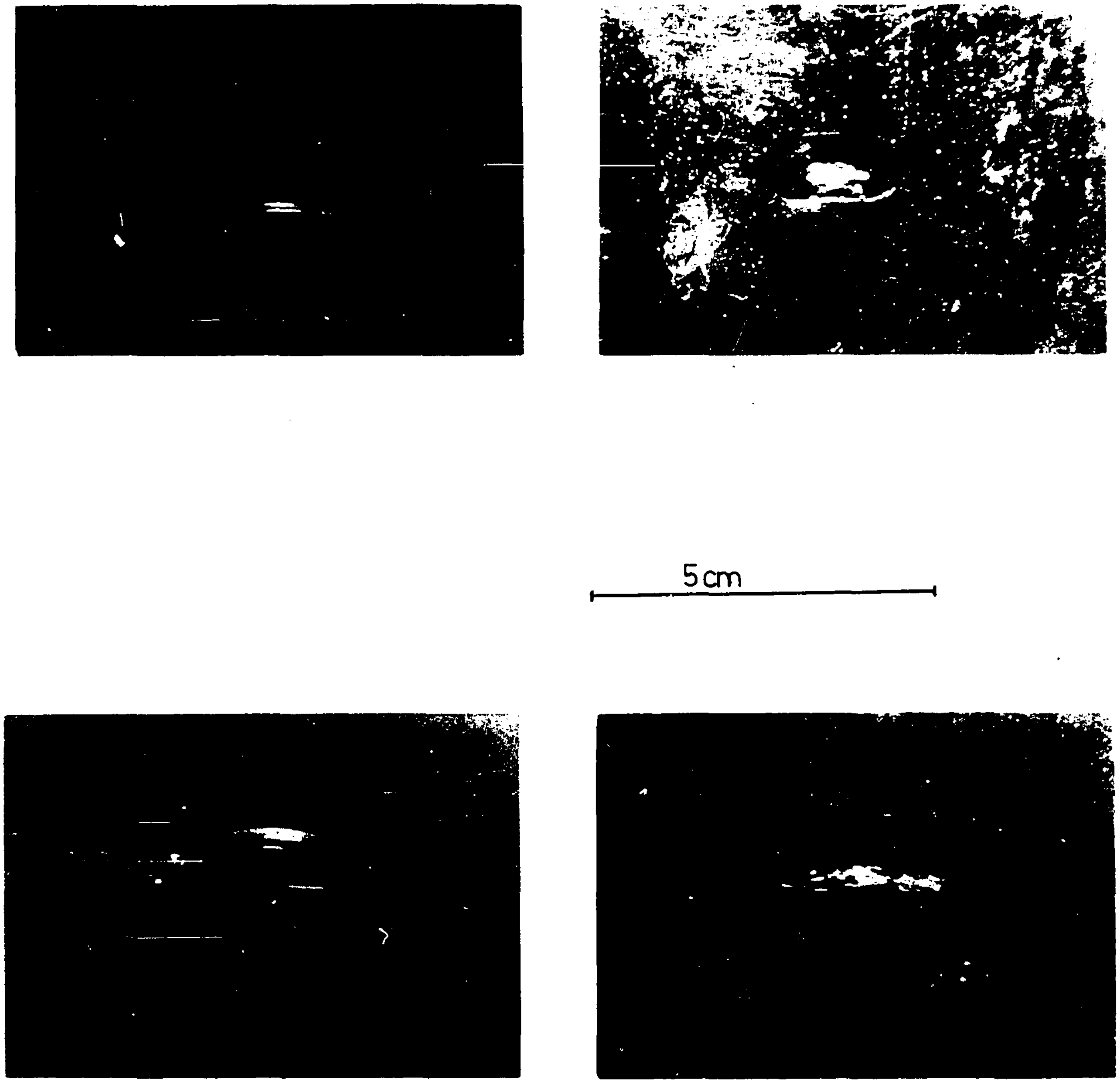

Figure 2.2-2 Bubbles Rising in Water (left) and in Mercury (right).

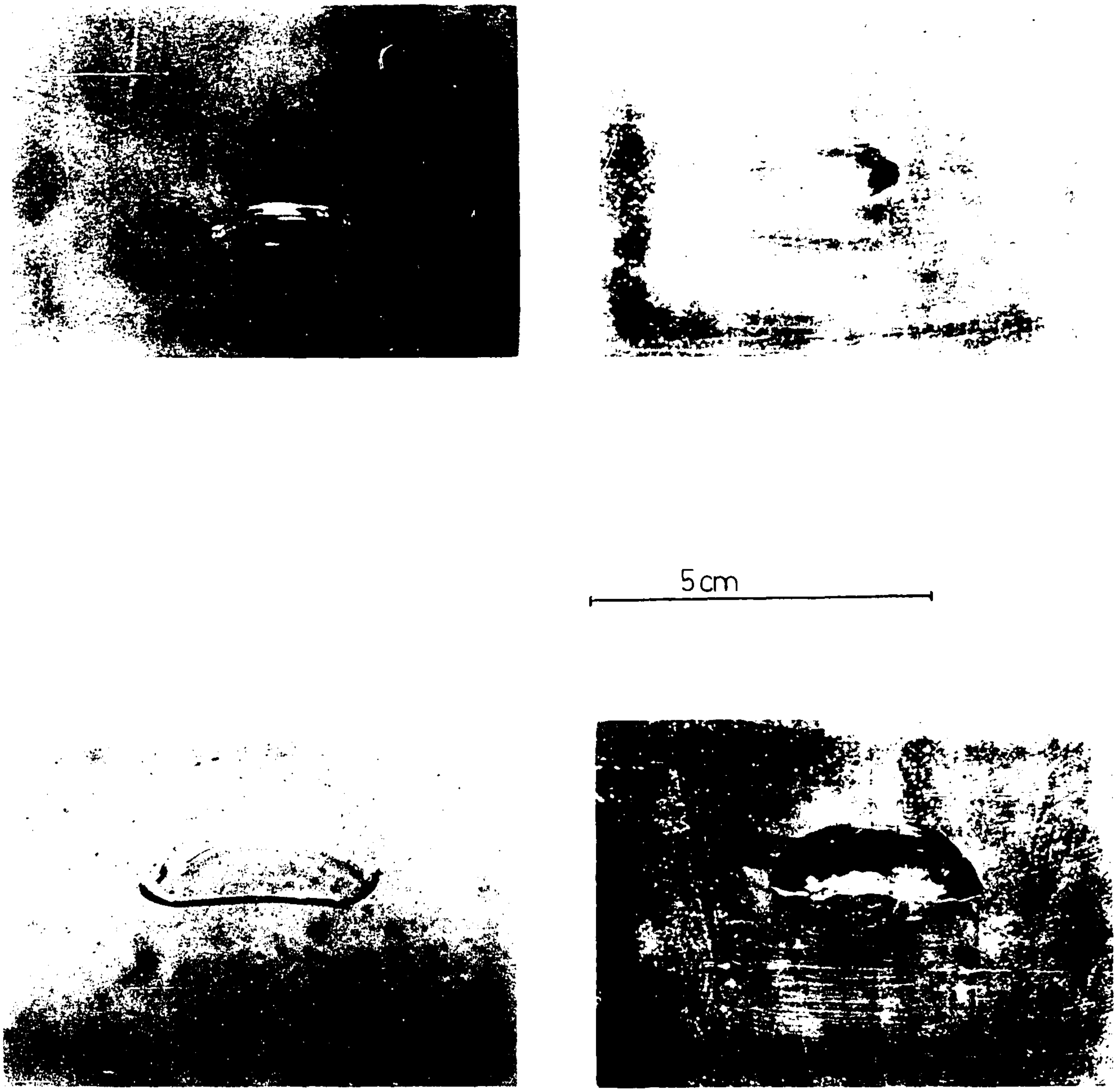

Figure 2.2-2 Bubbles Rising in Water (left) and in Mercury (right).

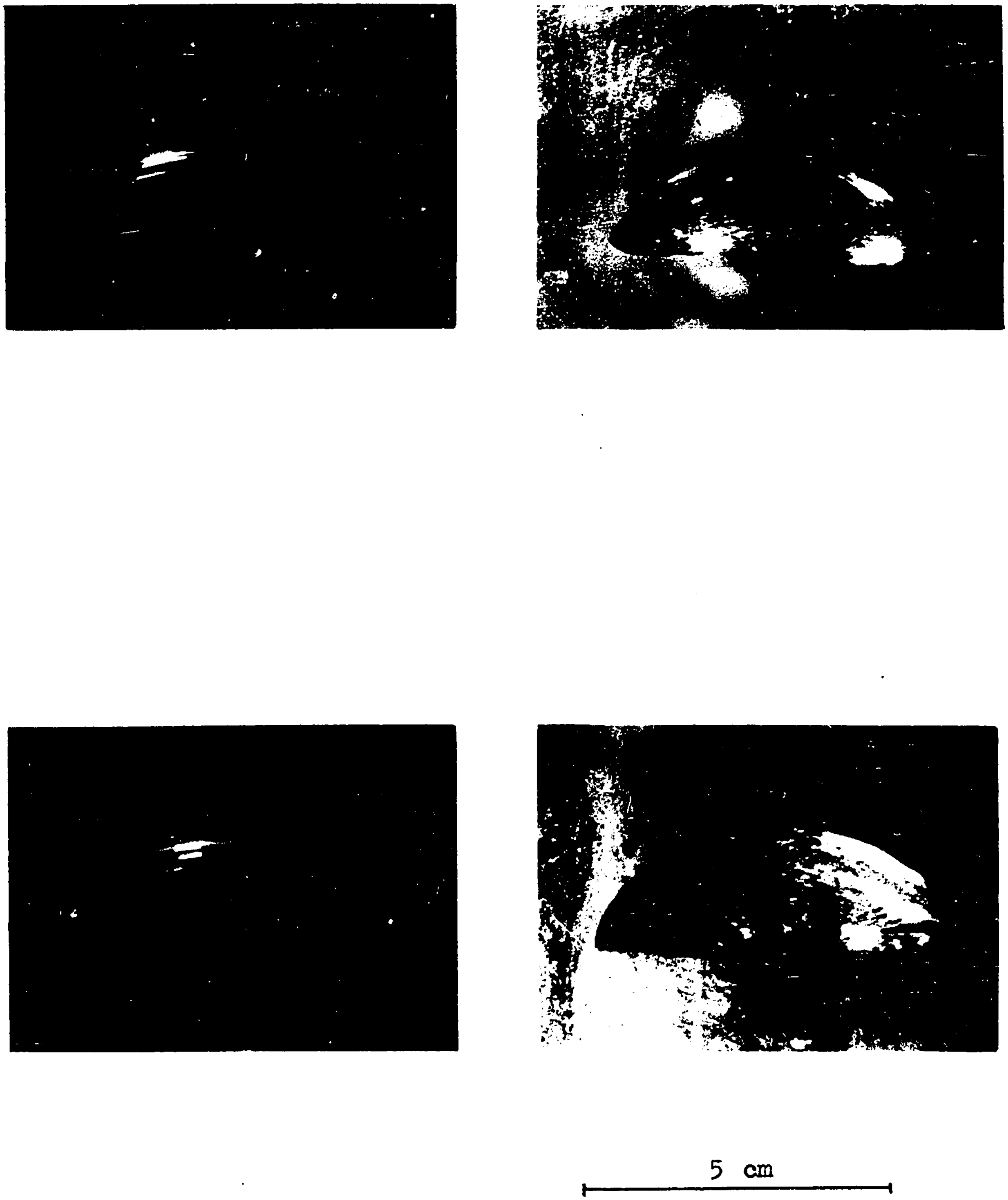

Figure 2.2-3 Bubbles Rising in Water (left) and in Mercury (right).

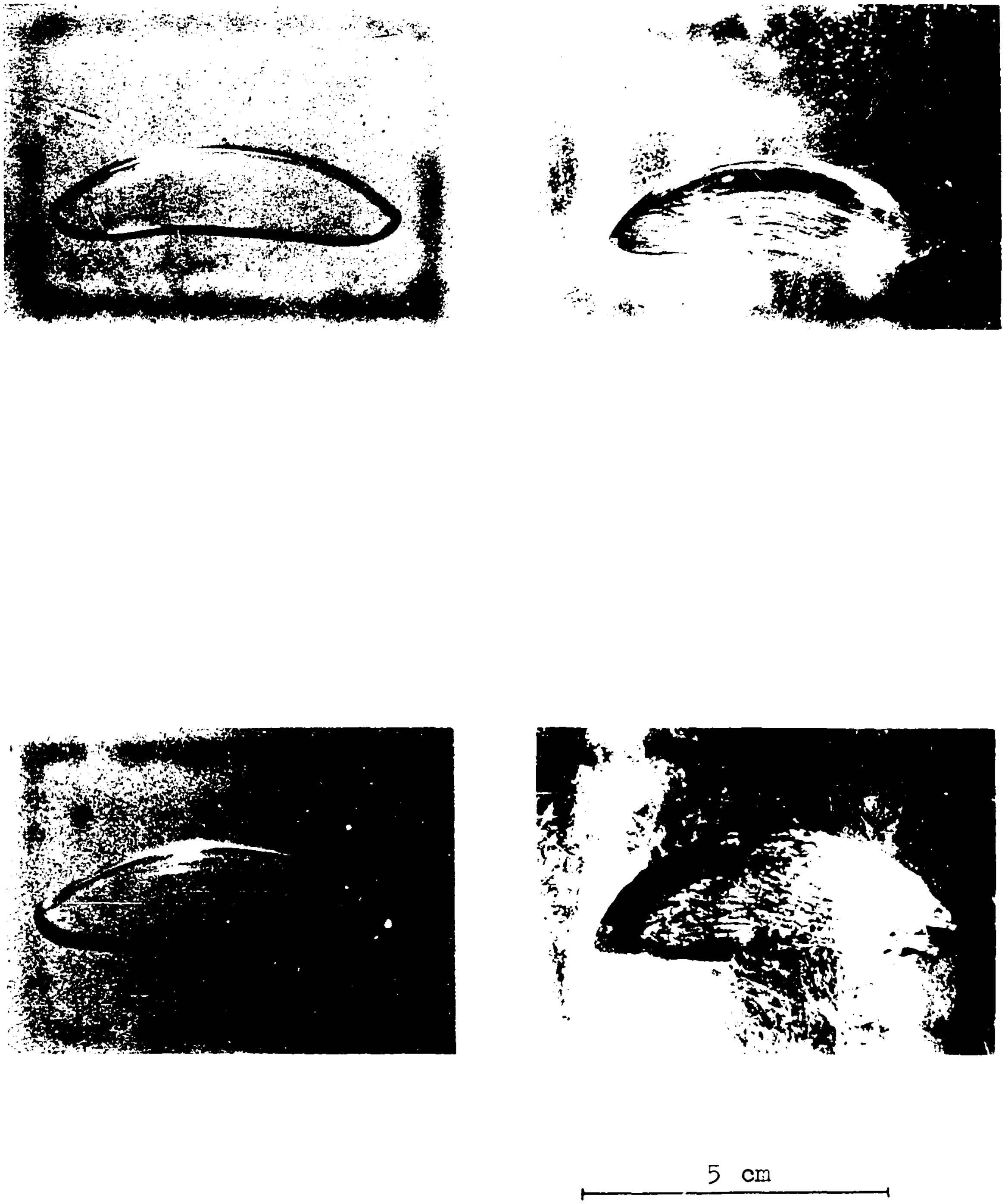

Figure 2.2-3 Bubbles Rising in Water (left) and in Mercury (right).

Table 2.2-1

Maximum Vertical (h) and Horizontal (w) Dimensions and Volume (V) of Single Bubbles Rising in Mercury (0.47 cm Thick Sheet).

w (cm)	h (cm)	w/h (-)	V (cm^3)
Photographed 30 cm above Cup			
2.80	0.95	2.83	1.60
3.00	1.05	2.85	1.75
3.85	1.30	2.97	2.00
4.05	1.43	2.80	3.20
4.35	1.50	2.90	3.50
4.40	1.50	2.93	3.60
4.55	1.50	3.03	3.80
4.60	1.63	2.83	4.10
4.60	1.70	2.70	5.50
5.04	1.75	2.90	5.80
5.40	1.90	2.84	6.20
5.50	1.80	3.06	6.30
5.60	1.80	3.10	6.60
5.60	2.00	2.80	6.80
5.66	1.90	2.97	6.80
5.80	1.95	2.96	6.80
5.80	1.90	3.05	6.80
5.86	2.05	2.85	6.80
6.06	2.00	3.03	6.90
6.16	2.15	2.86	6.90

Table 2.2-1 (Cont'd)

w (cm)	h (cm)	w/h (-)	V (cm^3)
Photographed 40 cm above Cup			
4.00	1.50	2.67	2.10
4.00	1.21	2.86	2.00
4.40	1.60	2.76	5.30
4.70	1.70	2.76	5.80
5.10	1.80	2.83	6.50
5.30	1.60	3.32	6.60
5.40	1.70	3.17	6.60
5.50	1.85	2.97	6.60
5.60	1.85	3.02	6.60
5.80	1.80	3.20	6.70
6.60	2.20	3.00	6.90
6.60	2.20	3.00	6.90
7.20	2.35	3.06	6.90

Table 2.2-1 (Cont'd)

w (cm)	h (cm)	w/h (-)	V (cm^3)
Photographed 50 cm above Cup			
2.00	0.67	2.98	0.41
2.10	0.72	2.91	0.82
2.50	0.80	3.12	1.03
3.00	1.00	3.00	1.75
3.00	1.00	3.00	1.50
3.50	1.17	3.00	1.75
3.60	1.20	3.00	2.90
3.60	1.25	2.88	1.95
4.20	1.40	2.99	3.49
4.30	1.39	3.10	3.00
4.70	1.60	2.93	4.28
4.90	1.60	3.06	3.92
5.10	1.68	3.10	6.08
5.30	1.75	3.03	4.37
5.30	1.80	2.93	6.50
5.40	1.82	2.97	6.49
5.50	1.83	3.01	6.20
6.00	2.03	2.96	5.87

Table 2.2-2

Maximum Vertical (h) and Horizontal (w) Dimensions and Volume (V) of Single Bubbles Rising in Water (0.47 cm Thick Sheet).

w (cm)	h (cm)	w/h (-)	V (cm^3)
Photographed 40 cm above Cup			
0.90	0.32	2.82	0.20
1.67	0.67	2.83	0.45
2.30	0.85	2.72	0.80
2.80	0.95	2.83	1.10
2.95	1.00	2.95	1.20
3.00	1.05	2.85	1.30
3.15	1.02	3.03	1.35
3.30	1.05	3.15	1.30
3.80	1.30	2.85	1.40
3.85	1.30	2.97	1.50
4.00	1.40	2.87	1.40
4.10	1.25	3.23	1.45
4.10	1.20	3.42	1.40
4.20	1.35	3.10	1.50
4.35	1.50	2.90	1.50
4.40	1.50	2.93	1.45
4.55	1.50	3.03	1.50
4.60	1.50	3.06	1.60
4.70	1.50	3.10	1.60
4.80	1.60	3.00	1.90
5.00	1.60	3.12	2.00

Table 2.2-2 (Cont'd)

w (cm)	h (cm)	w/h (-)	V (cm^3)
Photographed 50 cm above Cup			
1.70	0.57	3.01	0.30
1.80	0.60	3.00	0.40
2.20	0.75	2.93	0.50
3.00	1.02	2.97	1.00
3.30	1.05	3.14	1.10
3.30	1.10	3.00	1.30
3.50	1.10	3.16	1.40
3.50	1.12	3.15	1.00
4.00	1.28	3.12	1.30
4.50	1.45	3.10	1.50
4.50	1.48	3.03	1.60
4.50	1.50	3.00	1.50
4.80	1.52	3.16	1.60
4.80	1.60	3.00	2.00
5.00	1.60	3.13	1.90
5.20	1.64	3.17	2.10
5.30	1.70	3.12	2.50
5.30	1.75	3.02	2.60
5.50	1.75	3.14	2.40
5.50	1.75	3.14	3.00
5.60	1.80	3.11	2.60
5.70	1.70	3.35	3.10
5.80	1.85	3.13	3.10

B Rising Velocities

Velocities of single bubbles rising in mercury and in water are reported in Tables 2.2-3 and 2.2-4.

i) Water

In water experiments the volume of gas in the cup was directly measured by displacement measurement in the soap film meter. Bubble volumes and maximum vertical and horizontal dimensions in Table 2.2-3 are at the mid point of the distance over which velocities were measured.

ii) Mercury

Surging of the gas while filling the cup in the mercury experiments made direct measurement of initial volume (volume of the gas in the cup) difficult. It was possible, however, to accurately measure the change in volume ΔV during rise from the cup to the mercury surface.

The volume at any depth in the mercury could be calculated from cup depth and ΔV using the ideal gas law (i.e.):

$$V_t P_t = V_c P_c \qquad \text{Eq. 2.2-1}$$

and

$$V_t = V_c + \Delta V \qquad \text{Eq. 2.2-2}$$

Where V_t, P_t are volume and pressure at the upper surface of the mercury and V_c, P_c are volume and pressure in the cup.

Combining Equation 2.2-1 and Equation 2.2-2:

$$V_c = \frac{\Delta V}{(P_c/P_t - 1)} \qquad \text{Eq. 2.2-3}$$

The volume of the bubble (V_B) at any point in the liquid is given by:

$$V_B = \frac{\Delta V}{P_B(1/P_t - 1/P_c)} \qquad \text{Eq. 2.2-4}$$

where P_B is the pressure on the bubble.

In the case of rising bubbles each pressure can be related to the depth below the surface of mercury by:

$$P = 1 + \rho g Z \qquad \text{Eq. 2.2-5}$$

where Z is the depth below the surface.

Table 2.2-3

Width (w), Height (h), Volume (V) and Velocities (U) of Bubbles in a 0.47 cm Sheet of Water. (Velocities measured between 30 cm and 50 cm above release)

w (cm)	h (cm)	w/h (-)	V(cm^3)	U(cm/sec)
1.72	0.58	2.96	0.40	19.40
2.40	0.80	3.00	0.60	21.50
2.70	0.87	3.10	0.70	22.20
2.70	0.90	3.00	0.80	22.70
3.00	1.02	2.97	1.00	24.00
3.20	1.05	3.05	1.10	24.00
4.50	1.45	3.10	1.50	25.00
4.50	1.50	3.00	1.60	25.50
4.80	1.60	3.00	2.00	26.90
4.86	1.60	3.04	1.80	25.60
4.94	1.67	2.96	2.00	27.80
5.00	1.60	3.13	1.90	26.40
5.30	1.70	3.12	2.50	28.70
5.50	1.75	3.14	2.30	28.00
5.55	1.75	3.17	3.00	30.00

Table 2.2-4

Width (w), Height (h), Volume (V) and Velocities (U) of Bubbles rising 0.47 cm in a Sheet of Mercury. (Velocities measured between 30 cm and 50 cm above release)

w (cm)	h (cm)	w/h (-)	V (cm^3)	U(cm/sec)
2.00	0.67	2.98	0.41	22.10
2.10	0.72	2.91	0.82	22.40
2.50	0.80	3.12	1.03	24.80
3.00	1.00	3.00	1.75	24.60
3.00	1.00	3.00	1.50	23.60
3.50	1.17	3.00	1.75	25.70
3.60	1.20	3.00	2.90	29.20
3.60	1.25	2.88	1.95	27.20
4.20	1.40	2.99	3.49	27.40
4.30	1.39	3.10	3.00	29.20
4.70	1.60	2.93	4.28	28.80
4.90	1.60	3.06	3.92	30.00
5.10	1.68	3.10	6.08	29.20
5.30	1.75	3.03	4.37	29.60
5.30	1.80	2.93	6.50	29.90
5.40	1.82	2.97	6.49	30.00
5.50	1.83	3.01	6.20	30.20
6.00	2.03	2.96	5.87	31.00

2.3 DISCUSSION: ROOM TEMPERATURE INVESTIGATION

A Rising Velocities

Rising velocities in mercury and water sheets (Tables 2.3-1 and 2.3-2) are plotted in Figure 2.3-1 as a function of radius of curvature of the bubble (Figure 2.3-1, b). For comparison the $U = 2/3\ (g\ R_c)^{1/2}$ Davies and Taylor(11) expression for rise in a three dimensional environment and the Collins(13) expression for two dimensional rise $U = 1/2\ (g\ R_c)^{1/2}$ are included.

Radii of curvature have been calculated from h and w assuming that the cap surface is cylindrical.

The measured velocities are in all cases higher than predicted by the two dimensional model of Collins (Equation 2.0-7) and in general the velocities fall between the three dimensional Davies and Taylor Equation 2.0-5 and Equation 2.0-7. This result is in agreement with experiments in a 0.64 cm thick water sheet(15) in which velocities 9% larger than Equation 2.0-6 are reported.

Velocities higher than predicted can be attributed to a partially three dimensional character of flow, that is flow down the face (or third dimension) of the bubble.

It became obvious during the work that at least one face of a rising bubble was covered with liquid. This fact was apparent when it was found that a bubble rising in mercury could not be seen through. Later tests with dyed water confirmed this result.

Table 2.3-1

Volume (V), Width (w), Height (h), Velocity (U), Equivalent Radius (r_e), Radius of Curvature (R_c) and Subtended Angle (α) of Single Bubbles Rising in a Water Sheet at Level 50 cm.

$V(cm^3)$	w(cm)	h(cm)	U(cm/sec)	r_e(cm)	R_c(cm)	α(deg)
0.40	2.25	0.76	19.40	0.67	1.34	54
0.60	2.50	0.85	21.50	0.73	1.35	67
0.70	2.85	0.94	22.20	0.82	1.55	67
0.80	3.00	1.00	22.70	0.87	1.62	67
1.00	3.50	1.20	24.00	1.02	1.86	70
1.10	3.30	1.05	24.00	0.92	1.79	67
1.50	4.50	1.45	25.00	1.30	2.46	67
1.60	4.30	1.44	25.50	1.25	2.32	63
1.80	4.80	1.60	25.60	1.39	2.61	67
1.90	4.90	1.65	26.40	1.45	2.65	67
2.00	5.00	1.70	26.90	1.46	2.69	68
2.50	5.60	1.85	28.70	1.63	3.04	67
2.30	5.40	1.70	28.00	1.51	3.00	64
2.00	5.00	1.65	27.80	1.44	2.71	68
3.00	5.60	1.85	30.00	1.65	3.04	67

Table 2.3-2

Volume (V), Width (w), Height (h), Velocity (U), Equivalent Radius (r_e), Radius of Curvature (R_c), Subtended Angle (α) of Single Bubbles Rising in a Mercury Sheet at Level 50 cm.

$V(cm^3)$	w(cm)	h(cm)	U(cm/sec)	r_e(cm)	R_c(cm)	α(deg)
3.00	4.30	1.39	29.20	1.22	2.41	63
2.90	3.60	1.25	29.20	1.07	1.92	68
4.28	4.70	1.60	28.80	1.36	2.51	70
6.08	5.10	1.68	29.20	1.49	2.87	63
6.49	5.40	1.82	30.00	1.61	2.92	68
5.87	6.00	2.03	31.00	1.75	3.26	67
3.49	4.20	1.40	27.40	1.21	2.28	67
6.20	5.50	1.83	30.20	1.58	2.98	59
1.75	3.50	1.17	25.70	1.05	2.02	60
1.65	3.00	1.00	24.60	0.90	1.62	67
1.03	2.50	0.80	24.80	0.72	1.37	66
1.95	3.60	1.20	27.20	1.05	1.95	67
0.41	2.00	0.67	22.10	0.60	1.08	68
0.82	2.10	0.72	22.40	0.62	1.12	70
1.50	3.00	1.00	23.60	0.86	1.62	68
4.37	5.30	1.80	29.60	1.55	2.86	68
6.60	5.30	1.75	29.90	1.52	2.87	68
3.92	4.90	1.60	30.00	1.40	2.67	67

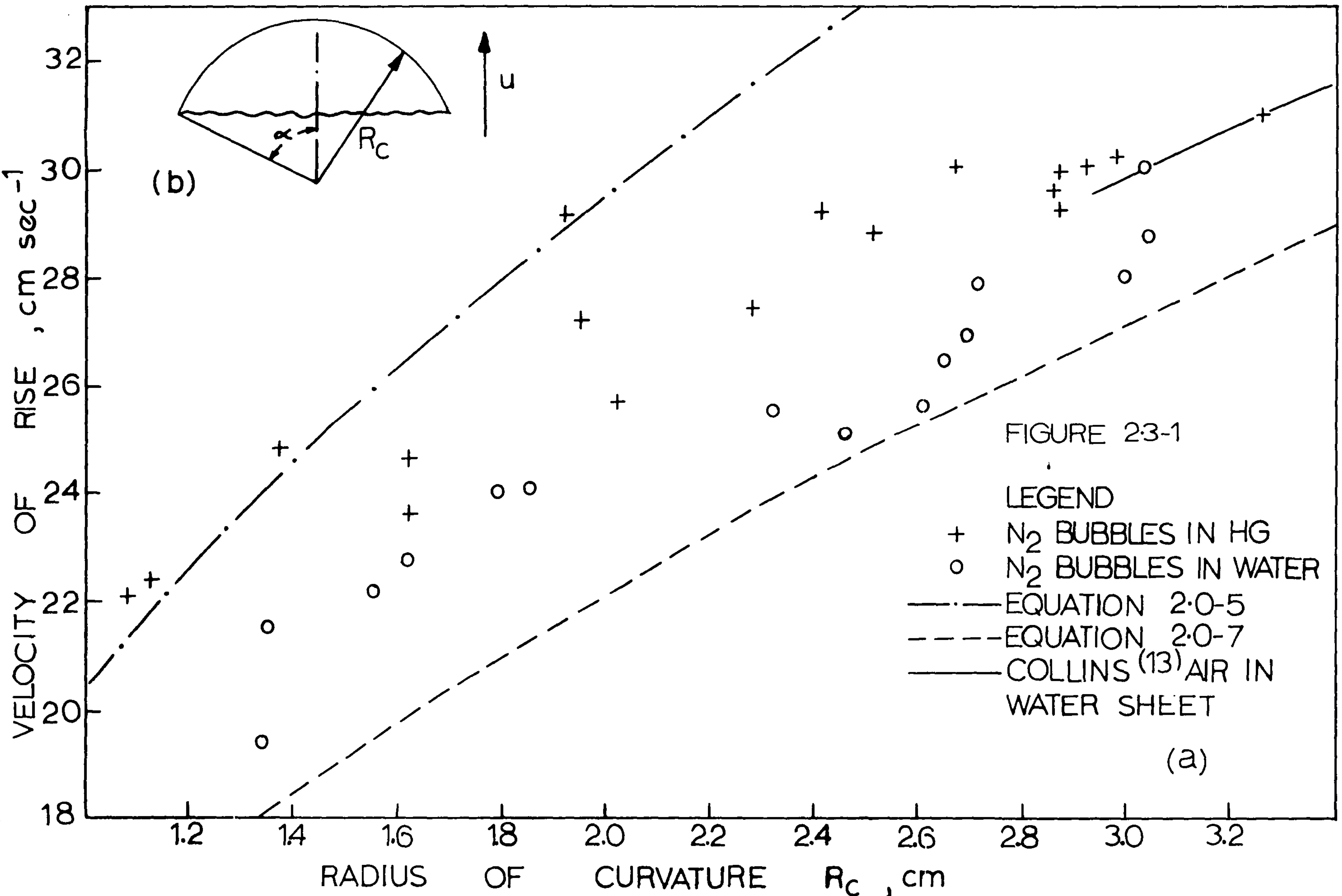
(b)
u
α
R_c
32
30
28
26
24
22
20
18
1.2
1.4
1.6
1.8
2.0
2.2
2.4
2.6
2.8
3.0
3.2
VELOCITY OF RISE , cm sec⁻¹
RADIUS OF CURVATURE R_c , cm
LEGEND
+ N₂ BUBBLES IN HG
o N₂ BUBBLES IN WATER
EQUATION 2·0-5
EQUATION 2·0-7
COLLINS (13) AIR IN WATER SHEET
(a)

FIGURE 2·3-1

In some cases during rise in mercury, especially at small volumes, both bubble faces would be covered making observation impossible. It was not always possible to predict which face of the bubble would be free of liquid but it seemed that for some reason (a coating of grease, for example) a preference for the liquid free face was developed.

Flow of liquid down the face of rising bubbles results in velocities tending toward the three dimensional rise equation (Equation 2.0-5).

This effect is accentuated at smaller volumes as the liquid film on the face is thicker. These bubbles are more three dimensional and more closely approach three dimensional flow conditions. When the diameter of the bubble becomes much less than the sheet thickness, the bubbles should behave as in a three dimensional liquid.

Velocities of bubbles rising in a sheet of mercury are 5 - 10 percent higher than those in a sheet of water. This result is a contradiction of the results of Davenport, Bradshaw, and Richardson(7) who showed that in a 15 cm diameter column of liquid, velocities in water and in mercury are virtually identical.

The higher velocities in mercury of the present are thought to be due to a delay in forming the stable cap shape after release from the cup. The nitrogen was observed to be in the form of an unstable "slug" just after release. This "slug" rises at velocities considerably higher than the cap shaped bubbles. Stabilization occurs much more quickly in water.

The reason for the delay in stabilization during rise in mercury is not clear (no delay is observed in water)(16) but the unstable behaviour may be likened to the rise of bubbles up vertical wires observed by Grace and Harrison(17). It is unlikely that surface tension forces are important as at a radius of 1 cm the surface tension pressure ($\frac{2\gamma}{R_c}$) is only 10^{-3} atmospheres compared with a total bubble pressure of 1½ atmospheres.

It appears that the gas first leaving the cup accelerates away from the remaining gas and that 20 to 30 cm of rise are required before the vertical stream of gas forms the stable cap shape. More sophisticated studies like the excellent experiments of Davidson and Walters(16) on the initiation of rise will be required before it is known whether liquid properties, cup rotation, or apparatus configuration are responsible for this behaviour.

B Shape of Bubbles

Shapes of cap bubbles are similar in sheets of water and mercury (Figure 2.2-3). Smaller bubbles pulsate rapidly but they appear to be the same shape in both liquids. This result confirms the similarity between water and mercury observed in earlier work(7) using electric probes in a column of liquid (Figure 2.0-4).

Shapes are also similar in 2 dimensional and 3 dimensional systems (Figure 2.3-2) but the angle subtended by the cap surface is larger in the two dimensional environment (α = 60° to 70°, Figure 2.3-3) than in the three dimensional environment (α = 45° to 60°)(5, 11)

The larger angles in two dimensional environment are consistent with the predictions of Collins (15) for rise in sheets of liquid and of Rippin and Davidson(12) for rise in columns of liquid. Each of these authors assumes:

(a) an infinite stagnant wake

(b) the velocity of fluid down the outside of the wake is the free stream (rising) velocity.

Application of these conditions to irrotational flow around a rising bubble leads to(12, 6) subtended angles of 60° in thin sheets of liquid and 50° in liquid columns.

These predicted values are within the range of the present experimental results.

The postulation of Davenport, Richardson and Bradshaw(9) that the trailing edge of spherical cap bubbles is more "rounded" in mercury due to the high surface tension forces is not borne out in the two dimensional system (Figure 2.2-3). The edges in mercury appear to be just as sharp as those in water.

An interesting result of the work is that the surfaces of the bubbles in mercury are rippled to a greater extent than in water (Figure 2.2-3). This rippling, if present

1. N_2 in Mercury Sheet

Scale: 5 cm

2. Air in 15 x 15 cm Column of Water

Figure 2.3-2

1. N_2 in Mercury Sheet

Scale: 5 cm

2. Air in 15 x 15 cm Column of Water

Figure 2.3-2

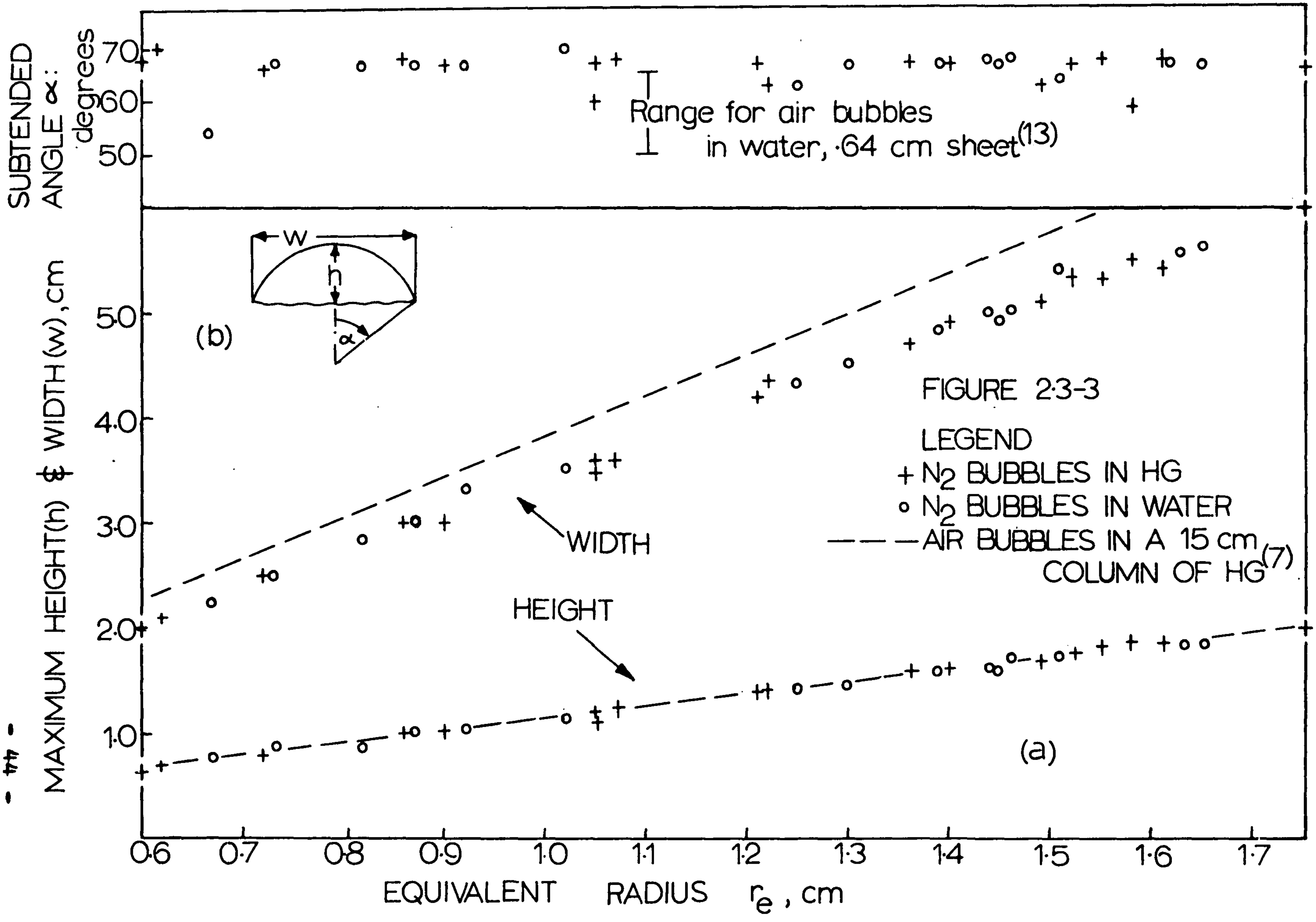

FIGURE 2·3-3

SUBTENDED ANGLE α : degrees
70
60
50
Range for air bubbles in water, ·64 cm sheet(13)
W
h
α
(b)
MAXIMUM HEIGHT(h) & WIDTH(w), cm
— h —
5.0
4.0
3.0
2.0
1.0
WIDTH
HEIGHT
(a)
LEGEND
+ N2 BUBBLES IN HG
o N2 BUBBLES IN WATER
— — — AIR BUBBLES IN A 15 cm COLUMN OF HG(7)
0·6
0·7
0·8
0·9
1·0
1·1
1·2
1·3
1·4
1·5
1·6
1·7
EQUIVALENT RADIUS re , cm

during rise in bulk liquid, will greatly enhance mass transfer rates between bubbles and liquid metals.

PART II

HIGH TEMPERATURE WORK: HYDROGEN REMOVAL FROM STEEL

3.0 PREVIOUS WORK: HIGH TEMPERATURE WORK-JET DEGASSING

Previous work on the removal of hydrogen from steel has been principally concentrated upon bubbling via submerged lances or porous plugs.

The experimental results of Spire(18), Houston and Death(19), and the British Iron and Steel Research Association(20) have shown that it is not possible to reduce the dissolved hydrogen level below 2-1/2 ppm by inert gas bubbling. This level is too high to guarantee a suitable steel product.

Model studies in oil and water suggest(20) that a high residual hydrogen content after argon bubbling is due to the intermixing of water bearing slag and metal as a result of the turbulence set up by the emerging bubbles.

The supposition of these authors is that slag/metal intermixing results in absorption of hydrogen from the slag (as water) into the metal.

Jet degassing overcomes this problem, however, by keeping a "blanket" of argon over the surface of the bath and by pushing the slag away to the bath edge.

Disadvantage of the Process

The major disadvantage of the jet process is that the surface area for reaction is very much smaller than the surface area provided by bubbles during lancing or during porous plug injection.

Previous studies(20-21) using high velocity jets have shown that gas efficiencies are of the order of 10% (i.e., the effluent gasses are only 10% saturated with hydrogen gas) as compared to 60% efficiencies reported by Houston and Death(19) for bubble degassing.

A summary of previous jet degassing work is shown on Table 3.0-1. As Table 3.0-1 indicates, studies of the use of jets have previously been restricted to characteristic velocities (gas flow rate (NTP)/bath surface area) in the order of 10 to 40 cm sec^{-1}.

In the present work, low velocity jets (characteristic velocity $\approx$0-0.3 cm sec^{-1}) have been used to determine:

(a) The lower limit of hydrogen concentration.

(b) The rate at which hydrogen can be removed.

At the outset of the present investigation it was proposed that the application of a low velocity jet combined with inert gas bubbling might result in the gas efficiencies of inert gas bubbling and the low residual hydrogen contents obtainable by the jet degassing technique.

Table 3.0-1

Argon Jet Degassing: Previous Work

Previous Investigations	Weight of Steel (lb)	Gas Flow Rate (ft^3 min^{-1})	Characteristic Gas Velocity* (cm sec^{-1})	Time (min)	Jets Number	Average Content of H_2 (ppm)	
						Before	After
Hoyle(20) (1962)	20	6 - 8	14 - 40	10-30	1	8.9	2.2
	80	10		10-20	7	6.5	1.5
Dewsnap(21) & Hoyle (1965)	20-780	5 - 7	14	10-20	19	4	1.4

* Total Argon Gas Flow Rate (NTP) ÷ Bath Surface Area

3.1 EXPERIMENTAL: HIGH TEMPERATURE WORK - JET DEGASSING

The degassing experiments were carried out on 5 kg melts of steel using a motor-generator induction furnace.

A Apparatus

(i) High Temperature Assembly (Figure 3.1-1)

An induction furnace,30 KW, 10 Kilocycle Tocco Meltmaster IB-20037-7-63 (Tocco Division - The Ohio Crankshaft Co., Cleveland, Ohio, U.S.A.) was employed. The steel was held in a zirconium oxide crucible 15 cm high and 14 cm internal diameter. The crucible was covered with silico-alumina refractory brick.

Argon was blown onto the molten steel via an alumina tube inserted vertically through a hole in the crucible cover.

(ii) Temperature Measurement and Control

The steel temperature was measured by an optical Pyrometer (Leeds & Northrup Co. Philadelphia). The temperature was maintained between 1550 and 1650°C by manual operation of the induction voltage rheostat.

B Materials

Steel: Commercial angle steel,
(0.20% C) Drummond McCall Co. Ltd.,
Montreal.

1. Pouring Spout & Top Seal
2. Top Board
3. Coil Terminals & Water Conn.
4. Encapsulated coil ass'y
5. Preformed crucible
6. Rammed Lining
7. Refractory Base
8. Bottom Board
9. Pouring Handle
10. Release and Safety Switch
11. Silico-Alumina Refractory Lid
12. Alumina Lance (Argon Jet)

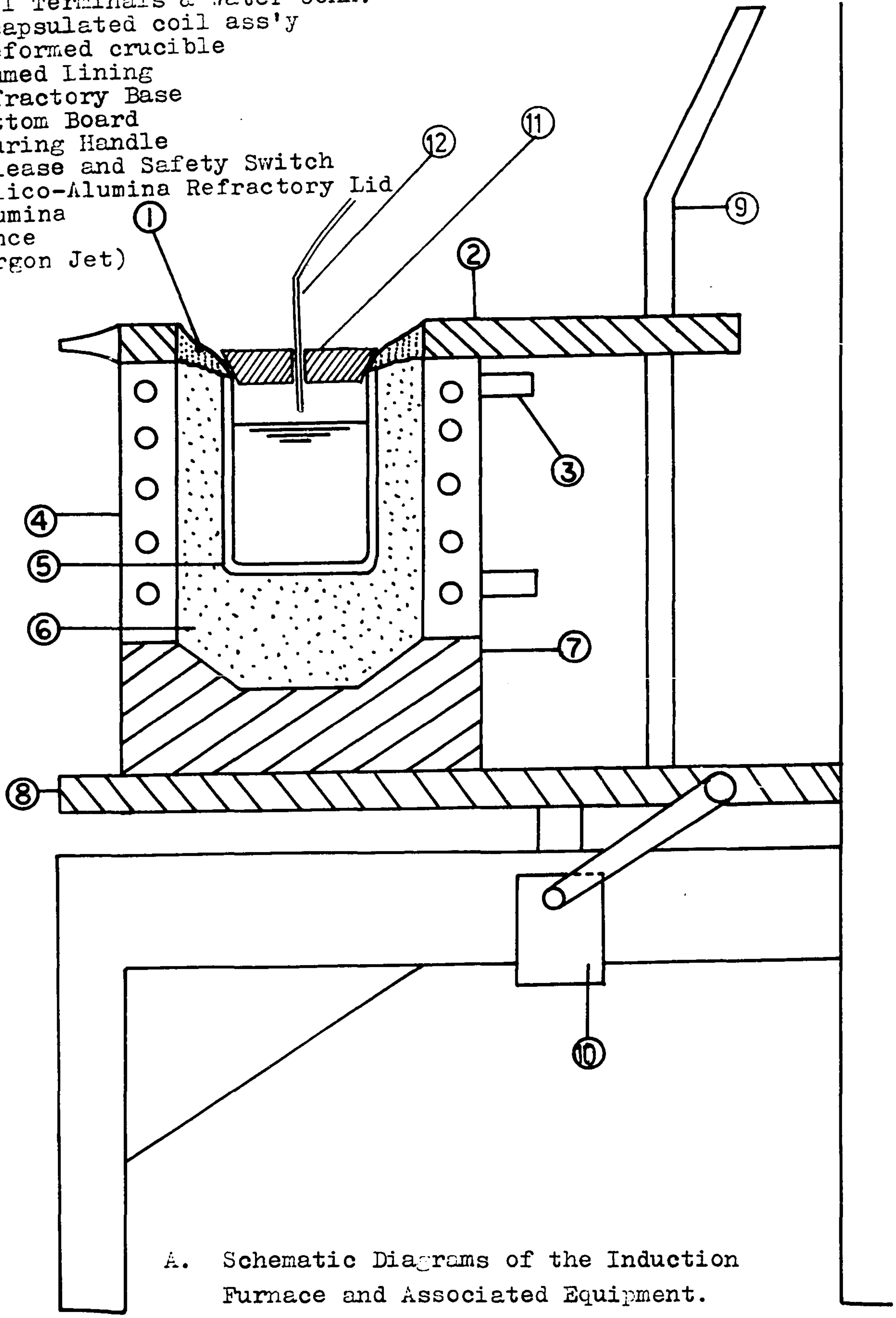

A. Schematic Diagrams of the Induction Furnace and Associated Equipment.

Fig. 3.1-1

Argon: Superpurified
99.997% Ar
2 ppm O_2
Dew Point: 76°F
Canadian Liquid Air, Limited,
Montreal

Hydrogen: Technical grade purified (99.995% H_2);
Canadian Liquid Air, Limited,
Montreal

C Hydrogen Analysis

(i) Analyser

The apparatus for the measurement of hydrogen content in steel (Cambridge Instrument Limited, Grosvenor Place, London, SW1) consisted of a furnace and a katharometer connected to form a closed loop in which gas circulates by thermal convection (Figure 3.1-2). The loop is initially filled with pure dry argon (Argon superpurified 99.997% Ar, Canadian Liquid Air).

The principle of the analysis is based upon the effusion of hydrogen from a heated metal sample and its detection by the katharometer.

After the analyser has been flushed with dry argon until a zero hydrogen content is indicated (usually 30 minutes), a sample is inserted into a trap chamber which is being flushed with dry argon.

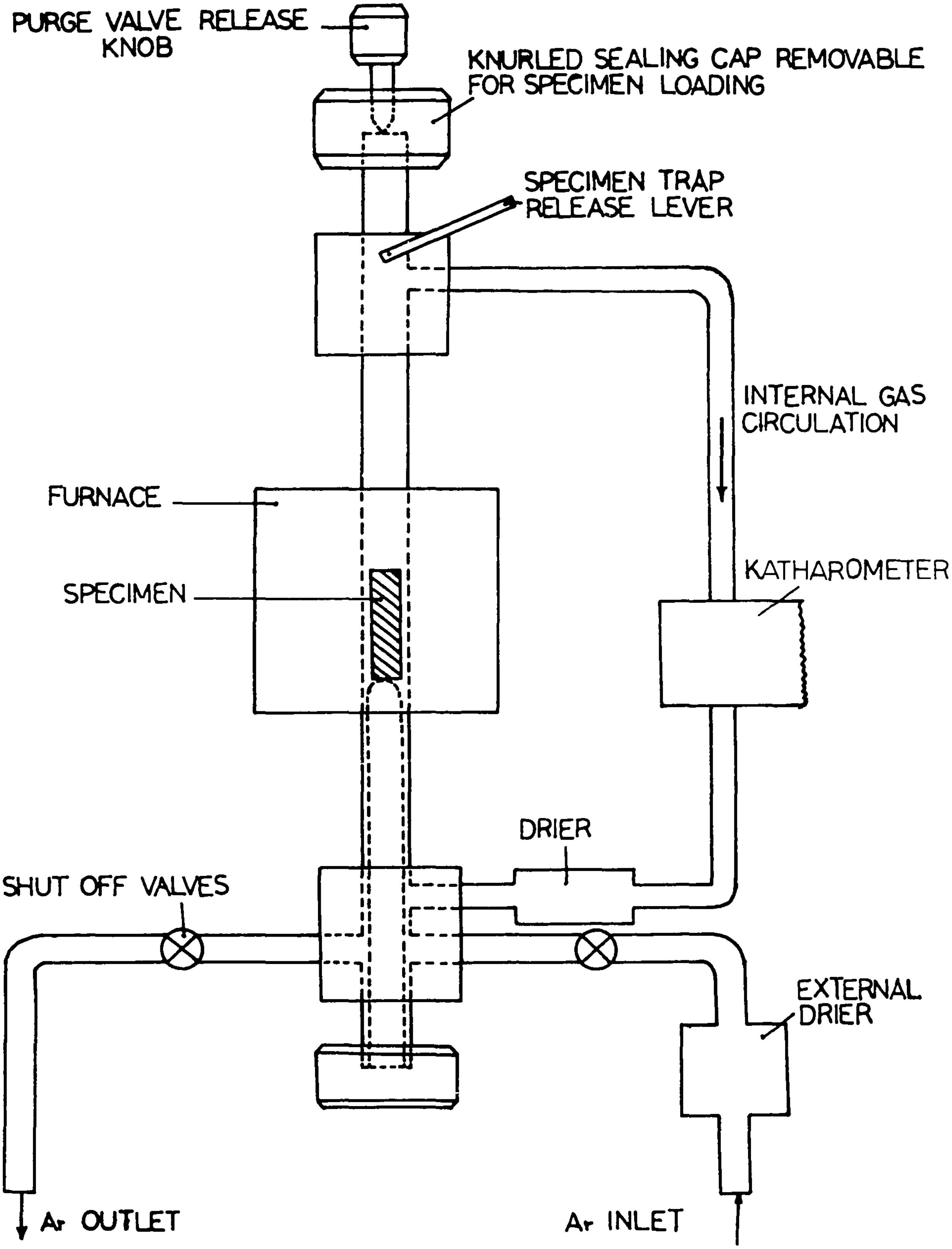

DIAGRAM OF THE GAS CIRCUIT IN THE ANALYSER
FIGURE. 3.1-2

The exit port of the trap is then sealed. The inlet and outlet valves of the loop are closed and the specimen is allowed to fall into the furnace (650°C) by means of a release lever.

The hydrogen effuses from the heated sample into the gas loop where its concentration (in argon) is measured by the katharometer.

The hydrogen concentration is registered on a conductivity bridge and potentiometer.

A steady reading representing the final detectable amount of hydrogen is obtained after about 15 minutes.

The amount of hydrogen in the sample is calculated from the percentage of hydrogen in the argon and the known volume of the analyser loop.

(ii) Sampling Techniques

Samples of steel were withdrawn from the molten bath into a pyrex tube (7 mm ID) using a suction bulb.

The samples were rapidly quenched in water or liquid nitrogen then placed in a solution of dry ice and acetone for low temperature storage.

During analysis, samples were immediately transferred from the cold storage into the analyser to avoid hydrogen loss.

Sources of error in the sampling technique can be described as follows:

1. Hydrogen may be lost from the sample as it solidifies and cools to the quench liquid temperature.
2. Hydrogen may be lost during cutting of the sample due to localized heating.
3. Hydrogen may be lost during storage prior to analysis. This loss was minimized by storing the samples at a low temperature for the shortest possible time.

Most of the experiments gave reproducible results and the total error was considered to be less than ± 1 ppm. When very scattered values were obtained the experiment was repeated.

D Method of Introduction of Hydrogen into Steel

The experimental study of hydrogen removal from steel consisted of partially saturating the steel with hydrogen followed by degassing with argon. In practice the hydrogen was introduced into the molten steel by impinging a jet of hydrogen, hydrogen and water vapour, or air and water vapour onto the surface of the molten steel.

Concentrations of up to 8 ppm hydrogen were obtained by this technique.

E General Experimental Procedure

5 Kg of commercial angle steel were placed into the crucible, the crucible was covered, and maximum power

(17 KVA) was applied to the induction coils. The steel became molten in about half an hour.

Samples of the steel were taken, and a single jet of hydrogen, or as in later experiments hydrogen or air saturated with water vapour, was directed vertically onto the steel surface.

These gases were blown onto the surface for a period of 10 to 30 minutes.

F Degassing Procedure

Hydrogen was removed from the partially saturated steel by impinging a jet of argon on the surface of the steel.

A single lance 0.8 cm ID was held vertically above the steel surface with the tip of the lance 2.5 cm ± 0.5 cm above the steel. The lance was introduced into the crucible through a loosely fitting refractory lid.

Argon flow rate was measured using a "Precision Bore Flowrator" (Labcrest, Fischer and Porter Co., Warminster, Pa.) rotameter type flowmeter. Flow was controlled by a needle valve at the gas regulator. The flowrate was varied between 0.0 cm^3 sec^{-1} and 50.0 cm^3 sec^{-1}.

Samples were taken prior to the impingement of argon on the surface and at 5 minute intervals during the course of the degassing.

3.2 RESULTS: HIGH TEMPERATURE INVESTIGATION

Five successful rate experiments were completed during the hydrogen removal study.

The main difficulty with the experimentation was absorbing enough hydrogen into the melt prior to the degassing trials. Sampling and analysis for hydrogen leads to accuracies in the order of ± 1 ppm so that degassing runs required at least 5 ppm hydrogen at the start of degassing to obtain meaningful variations in degassing rates.

Initial hydrogen concentrations in the order of 8 ppm were finally obtained by impinging a jet of water saturated H_2 or water saturated air onto the surface of the steel.

The results of the degassing tests are tabulated in Tables 3.2-1 to 3.2-5 and plotted in Figure 3.2-1.

A Mass Transfer Coefficients

The experimental results have been interpreted in terms of the liquid phase mass transfer coefficient α_L defined by:

$$\frac{dn_H}{dt} = - \alpha_L \; A_S \; (C^{bL}_H - C^{sL}_H) \qquad \text{Eq. 3.2-1}$$

In the process of effusion of a gas from a liquid in which the molecularity of the effusing species is unchanged (i.e., CO_2 in water, CO_2 in air) the effusion process can be considered (where chemical reaction rate at the interface is fast)

Table 3.2-1

Flow Rate of Argon:	50.00 cm^3 sec^{-1}
Characteristic Velocity (Flow Rate/Bath Area):	0.32 cm sec^{-1}
Mass of Steel:	5 Kg
Temperature:	1600°C
Size of Gas Jet Tube:	0.8 cm ID
Distance of Jet from Metal Surface:	2.5 cm
Size of Depression in Metal Surface:	0.3 cm ± 0.1 cm

Time (min.)	Sample Number	Hydrogen Concentration (ppm)
0	1	5.2
0	2	4.7
0	3	4.9
0	4	5.2
5	1	1.2
5	2	1.2
5	3	1.0
5	4	1.6
10	1	1.0
10	2	0.9
10	3	0.9
10	4	1.0
15	1	0.7
15	2	0.9
15	3	0.8
15	4	0.7

Table 3.2-2

Flow Rate of Argon:	50.00 cm^3 sec^{-1}
Characteristic Velocity (Flow Rate/Bath Area):	0.32 cm sec^{-1}
Mass of Steel:	5 Kg
Temperature:	1600°C
Size of Gas Tube:	0.8 cm ID
Distance of Jet from Metal Surface:	2.5 cm
Size of Depression in Metal Surface:	0.3 cm ± 0.1 cm

Time (min.)	Sample Number	Hydrogen Concentration (ppm)
0	1	7.2
0	2	5.6
0	3	6.5
5	1	2.0
5	2	2.0
5	3	2.4
10	1	1.5
10	2	1.5
10	3	1.3
15	1	1.3
15	2	1.0
15	3	1.3
20	1	0.6
20	2	0.5
20	3	0.4

Table 3.2-3

Flow Rate of Argon: 40.00 cm^3 sec^{-1}
Characteristic Velocity (Flow Rate/Bath Area): 0.26 cm sec^{-1}
Mass of Steel: 5 Kg
Temperature: 1600°C
Size of Gas Tube: 0.8 cm ID
Distance of Jet from Metal Surface: 25 cm
Size of Depression in Metal Surface: 0.2 cm ± 0.1 cm

Time (min.)	Sample Number	Hydrogen Concentration (ppm)
0	1	6.7
0	2	7.1
0	3	7.4
0	4	7.7
5	1	3.2
5	2	2.9
5	3	3.0
10	1	1.5
10	2	1.6
10	3	1.9
10	4	2.1
15	1	1.3
15	2	1.2
15	3	1.5
15	4	1.4

Table 3.2-4

Flow Rate of Argon:	25.00 $cm^3 sec^{-1}$
Characteristic Velocity (Flow Rate/Bath Area):	0.16 $cm\ sec^{-1}$
Mass of Steel:	5 Kg
Temperature:	1600°C
Size of Gas Tube:	0.8 cm ID
Distance of Jet from Metal Surface:	25 cm
Size of Depression in Metal Surface:	0.1 cm ± 0.05 cm

Time (min.)	Sample Number	Hydrogen Concentration (ppm)
0	1	7.8
0	2	7.9
0	3	7.1
0	4	6.5
5	1	4.1
5	2	5.8
5	3	4.1
10	1	2.6
10	2	1.5
10	3	4.0
15	1	1.3
15	2	1.4
15	3	2.8

Table 3.2-5

Flow Rate of Argon:	0.00 cm^3 sec^{-1}
Characteristic Velocity (Flow Rate/Bath Area):	0.00cm sec^{-1}
Mass of Steel:	5 Kg
Temperature:	1600°C
Size of Gas Tube:	0.8 cm ID

Time (min.)	Sample Number	Hydrogen Concentration (ppm)
0	1	7.8
0	2	8.2
0	3	9.0
0	4	7.9
5	1	5.9
5	2	6.5
5	3	6.4
5	4	6.4
10	1	5.7
10	2	4.9
10	3	4.9
10	4	4.3
15	1	3.7
15	2	4.4
15	3	4.3
15	4	4.9

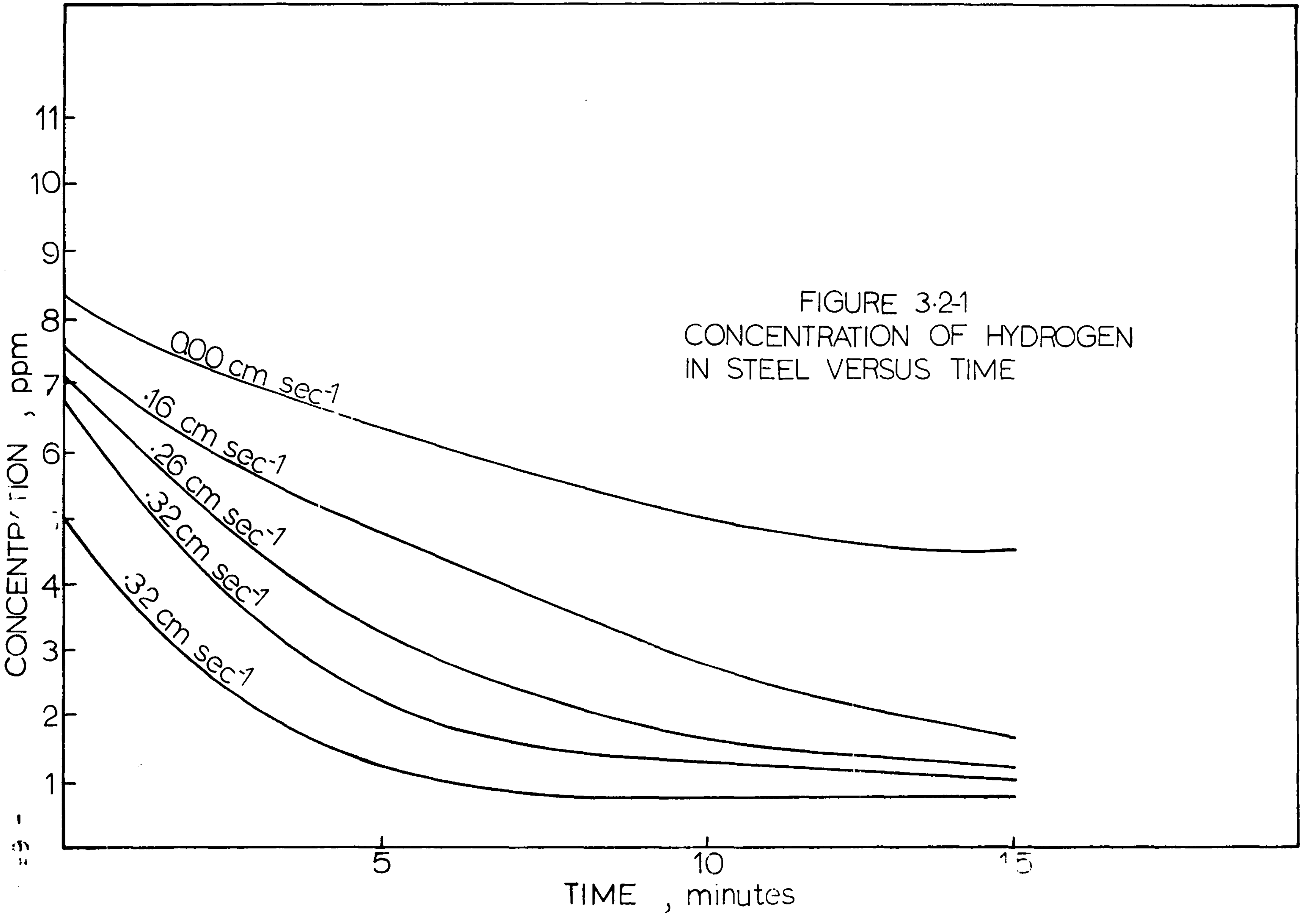

FIGURE 3·2-1
CONCENTRATION OF HYDROGEN
IN STEEL VERSUS TIME

in terms of an overall mass transfer coefficient α_o defined by:

$$\frac{dn_{CO_2}}{dt} = -\alpha_o A \left(C^{bL}_{CO_2} - FP^{bg}_{CO_2}\right) \qquad \text{Eq. 3.2-2}$$

(F, Henry's Law coefficient)

where $$\frac{1}{\alpha_o} = \frac{1}{\alpha_L} + \frac{F}{\alpha_g} \qquad \text{Eq. 3.2-3}$$

In the case of a gas dissolved atomically effusing to form a diatomic gas, α_o is not, however, independent of concentration and is not, as a result, useful in interpreting or tabulating results.

It would, however, be equally valid to present the experimental effusion data in terms of a gas phase mass transfer coefficient defined by:

$$\frac{dn_H}{dt} = -2\alpha_g A_S \left(\frac{P^{sg}_{H_2}}{RT} - \frac{P^{bg}_{H_2}}{RT}\right) \qquad \text{Eq. 3.2-4}$$

rather than by the equation 3.2-1 liquid phase mass transfer coefficient.

B Comparison of Expected Effusion Rates: Liquid Phase or Gas Phase Control

Effusion rates for liquid phase and gas phase transport control can be predicted on the basis of existing transport models.

In general it can be shown that under identical fluid dynamic conditions mass transfer coefficients are proportional to the diffusion coefficient to between the 1/2(22, 23) and 1 power.(24)

Calculations of mass transfer coefficient which assume a concentration difference of 4 ppm in the liquid (liquid phase control) or an equivalent pressure gradient in the gas phase ($P_{H_2}^{sg} - P_{H_2}^{bg}$) of .022 atmospheres are shown in Table 3.2-6.

This pressure gradient is calculated from the equilibrium Sieverts relationship(25):

$$[H] \text{ ppm} = 27\, P_{H_2}^{1/2} \qquad \text{Eq. 3.2-5}$$

and is equivalent to a concentration difference between 4 ppm in the bulk metal and 0 ppm at the gas metal surface i.e., the P_{H_2}, $[H]$ relationship is not linear.

Table 3.2-6 shows that gas phase control cannot be eliminated from consideration but that, in fact, gas phase control may be the more important factor if a 1/2 power dependence on diffusion coefficient is shown.

Diffusion control in the liquid phase will be important in both models however, hence the results have been treated arbitrarily in terms liquid phase mass transfer coefficients, α_L.

C Chemical Reaction Rate Control

The preceding analysis assumes that the rate of reaction is controlled by hydrogen transport to and from the gas metal interface. This condition is equivalent to assuming equili-

Table 3.2-6

Relative Rates of Transport of Hydrogen in Liquid Phase and in Gas Phase

Data:

Temperature: 1600°C

$D_{[H]}$ in Fe: (25) 1.3×10^{-3} cm^2 sec^{-1}

$D_{[H_2]}$ in Ar(26): 11 cm^2 sec^{-1} (Estimated from D_{H_2} in air)

$C^{bL}_{[H]} - C^{sL}_{[H]} = 2.9 \times 10^{-5}$ g-atoms cm^{-3}

$\frac{1}{RT}(P^{sg}_{H_2} - P^{bg}_{H_2}) = 1.47 \times 10^{-7}$ g-atoms cm^{-3}

Model: Rate of Transport $\propto D^{1/2}$

$$\frac{\text{Rate of } H_2 \text{ Effusion (Liquid Phase Control)}}{\text{Rate of } H_2 \text{ Effusion (Gas Phase Control)}} = \frac{\frac{1}{2} D^{1/2}_{[H]} (C^{bL}_{[H]} - C^{iL}_{[H]})}{D^{1/2}_{H_2} \frac{1}{RT} (P^{sg}_{H_2} - P^{bg}_{H_2})}$$

$$= \frac{\frac{1}{2}(1.3 \times 10^{-3})^{1/2} (2.9 \times 10^{-5})}{(11)^{1/2} \quad (1.47 \times 10^{-7})} = 1.1 \ \frac{\text{Liquid Rate}}{\text{Gaseous Rate}}$$

∴ Rates approximately equal

Model: Rate of Transport $\propto D$

$$\frac{\text{Rate of } H_2 \text{ Effusion (Liquid Phase Control)}}{\text{Rate of } H_2 \text{ Effusion (Gas Phase Control)}} = \frac{\frac{1}{2} D_{[H]} (C^{bL}_{[H]} - C^{sL}_{[H]})}{D_{H_2} (\frac{1}{RT}) (P^{sg}_{H_2} - P^{bg}_{H_2})}$$

$$= \frac{\frac{1}{2}(1.3 \times 10^{-3}) (2.9 \times 10^{-5})}{11 \ (1.47 \times 10^{-7})} = 1.17 \times 10^{-2} \ \frac{\text{Liquid Rate}}{\text{Gaseous Rate}}$$

∴ The reaction is liquid phase controlled as the rate of transport in liquid is much lower than in the gas phase.

brium conditions at the interface, hence, an infinitely fast chemical reaction rate.

El-Tayeb and Parlee(25) in their experimental study of hydrogen absorption into the liquid steel showed that the volume of hydrogen absorbed (NTP) into a column of liquid iron should be:

$$V_{H_2} = \frac{d^2 \rho_m \; C_H^s \sqrt{\pi D t}}{200 \rho_g} \qquad \text{Eq. 3.2-6}$$

for a diffusion controlled reaction, i.e. volume absorbed should be proportional to exposure time. This $(t)^{1/2}$ relationship was in fact obtained experimentally by El-Tayeb and Parlee(25) thus strongly suggesting diffusion control.

These authors also report an activation energy of 3 Kcal per mole of hydrogen and suggest that this value is also indicative of a diffusion controlled process.

Although these two findings cannot be regarded as concrete proof that the hydrogen absorption is diffusion controlled, there is no evidence to suggest otherwise.

The process of desorption during hydrogen degassing would similarly be expected to be diffusion rather than chemically controlled. In this case (argon-hydrogen gas mixture) gas phase diffusion would be involved as described in section B.

D Experimental Mass Transfer Coefficient

Mass transfer coefficients have been calculated from the experimental degassing results from the definitional Equation 3.2-1. The procedure followed was to determine dn_H/dt for each experiment at t = 2, 5 and 10 minutes from slopes of hydrogen content in steel versus time curves (Figure 3.2-1).

Bulk hydrogen concentrations in the steel, C_H^{bL} were also obtained at the 2, 5 and 10 minute marks.

In establishing a value for the concentration of hydrogen in steel at the gas/steel interface, C_H^{sL}, two possibilities were considered:

(a) The hydrogen concentration in the argon at the steel interface was zero and hence C_H^{sL} was zero.

(b) The gas phase inside the covered crucible was completely and instantly mixed in which case the partial pressure of hydrogen in the gas phase at any instant is given by the ratio:

$$P_{H_2} = \frac{1/2 \ dn_H / dt}{\left(\dot{n}_{Ar} + 1/2 \ dn_H/dt\right)} \qquad \text{Eq. 3.2-7}$$

where $\dot{n}_{Ar}$ is the flow rate of the argon jet (moles sec^{-1}) and $\frac{dn_H}{dt}$ is the rate of hydrogen effusing from the steel.

Equation 3.2-7 is developed in Appendix 1 (Page 85)

Calculations of mass transfer coefficients were performed using the latter model with the justification that although the metal area immediately beneath the argon jet is exposed to pure argon, a majority of the metal surface is exposed to the argon-hydrogen mixture.

Values of C_H^{sL} were calculated from P_{H_2} assuming the equilibrium Sieverts(25) relationship:

$$[H]^s_{ppm} = 27 \left(P_{H_2}\right)^{1/2} \qquad \text{Eq. 3.2-8}$$

which is equivalent to the condition of no mass transfer resistance in the gas phase.

Figure 3.2-2 and Table 3.2-7 show the experimental values of α_L as a function of the time after the start of argon blowing and of flow rate. A trend toward higher mass transfer coefficient with increasing flow rate is evident. The trend is in accord with the expressions developed by Wakelin and Bradshaw(27) who show that under conditions of radial flow from a central jet:

$$\alpha_L = \text{const.} \; (\dot{n}_A \, D/r)^{1/2} \qquad \text{Eq. 3.2-9}$$

The constant depends upon the thickness of the radially moving gas layer.

Unfortunately, the present results are not sufficiently precise to test the validity of Equation 3.2-9 as the accuracy of the mass transfer coefficients, based upon the ± 1 ppm error in hydrogen analyses, can be considered to be in the order of $\pm 1 \times 10^{-2}$ cm sec^{-1}.

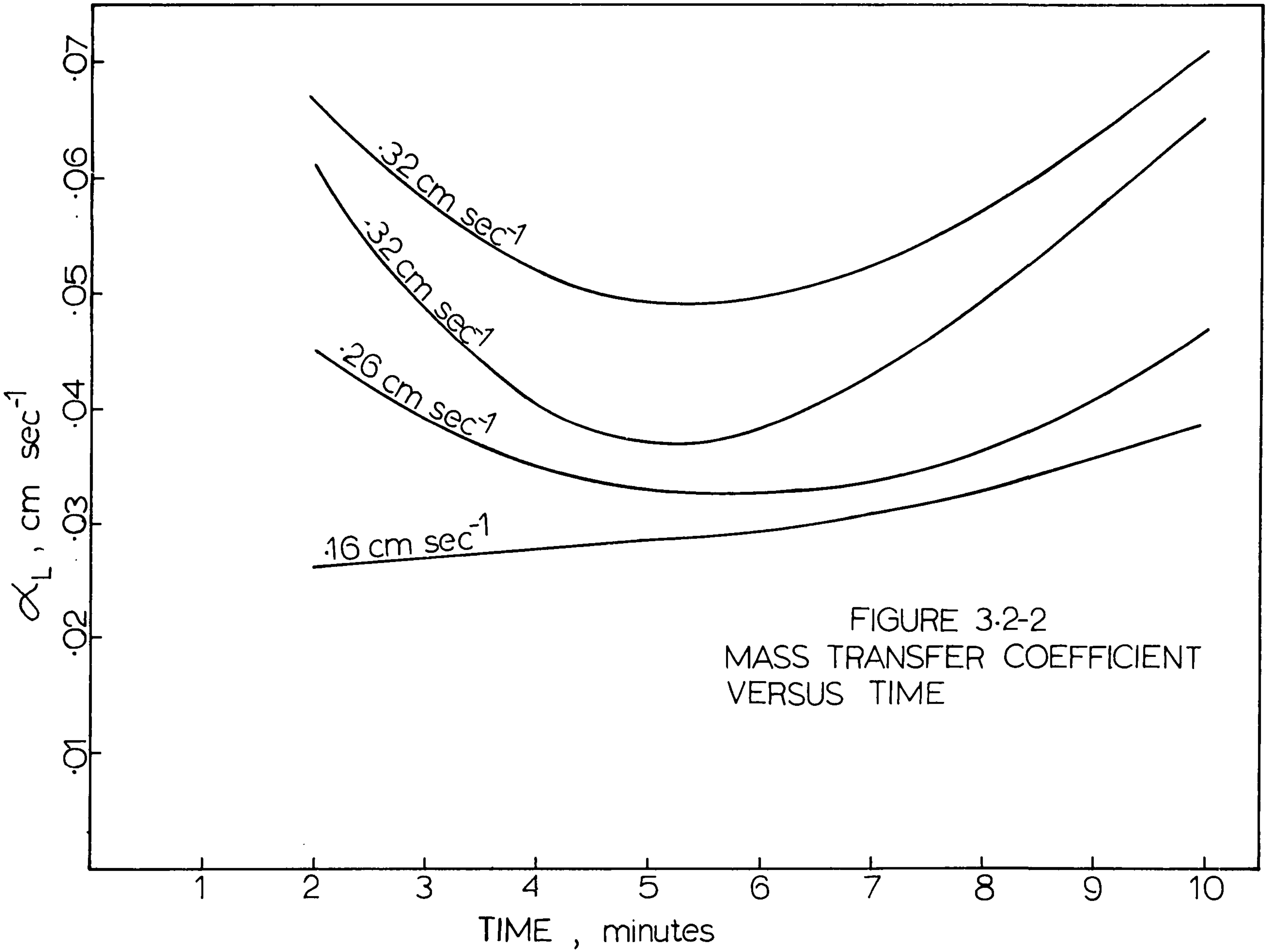

FIGURE 3·2-2
MASS TRANSFER COEFFICIENT
VERSUS TIME

Table 3.2-7
Mass Transfer Coefficient Calculations

Time (min)	Rate of Hydrogen Evolution $\frac{d[H]^b}{dt}$ (ppm min^{-1})	Hydrogen Pressure Eq. 3.2-7 P_{H_2} (atmos.)	Surface Hydrogen Concentration $[H]^s$ (ppm)	Bulk Hydrogen Concentration $[H]^b$ (ppm)	Mass Transfer Coefficient α_L (cm sec^{-1})
	Flow Rate: 25 cm^3 sec^{-1}; Characteristic Velocity: 0.16 cm sec^{-1}				
2	0.610	0.0222	4.05	5.80	0.026
5	0.425	0.0156	3.39	4.50	0.029
10	0.210	0.0078	2.40	2.80	0.039
	Flow Rate: 40 cm^3 sec^{-1}; Characteristic Velocity: 0.26 cm sec^{-1}				
2	0.800	0.0184	3.66	5.00	0.045
5	0.320	0.0070	2.25	3.00	0.033
10	0.142	0.0033	1.57	1.80	0.047
	Flow Rate: 50 cm^3 sec^{-1}; Characteristic Velocity: 0.32 cm sec^{-1}				
2	0.750	0.0138	3.16	4.00	0.067
5	0.230	0.0043	1.75	2.10	0.049
10	0.140	0.0026	1.37	1.51	0.071
	Flow Rate: 50 cm^3 sec^{-1}; Characteristic Velocity: 0.32 cm sec^{-1}				
2	0.500	0.0092	2.58	3.20	0.061
5	0.096	0.0017	1.11	1.30	0.037
10	0.052	0.00096	0.84	0.90	0.065

It can be seen, however, that a doubled flow rate (25 to 50 cm^3 sec^{-1}) raises the mass transfer coefficient by a factor of 2-1/2 at t = 2 minutes, and a factor of approximately 1-1/2 at t = 5 and 10 minutes. These values can be compared with the $\sqrt{2}$ factor predicted by Equation 3.2-6.

Mass transfer coefficients obtained from the present degassing results appear to vary with time (Figure 3.2-2) in opposition to constant values expected for well stirred systems. No satisfactory explanation for the α_L minima at 5 minutes of exposure has been developed. The variations are, however, within the accuracy range ($\pm$ .01 cm sec^{-1}) suggested for the mass transfer coefficient results.

An attempt to relate the present mass transfer results to earlier work of Wakelin(27) has been made by plotting mass transfer coefficient as a function of nozzle to liquid distance and jet momentum per unit surface area, Figure 3.2-3. Because Wakelin's data is for the system CO_2/water the present H_2/ steel results have been adjusted for diffusion coefficient using Equation 3.2-9.

i.e. $$\alpha_L = \alpha_{L_{H_2/Fe}} \left(\frac{D_{CO_2 \text{ in } H_2O}}{D_H \text{ in Fe}} \right)^{\frac{1}{2}}$$

Adjusted to CO_2/water results $$= \alpha_{L_{H_2/Fe}} \left(\frac{1.35 \times 10^{-5}\ (15°C)^{(25)}}{1.28 \times 10^{-3}\ (1550)^{(26)}} \right)^{\frac{1}{2}}$$

$$\cong .1\ \alpha_{L_{H_2/Fe}}$$

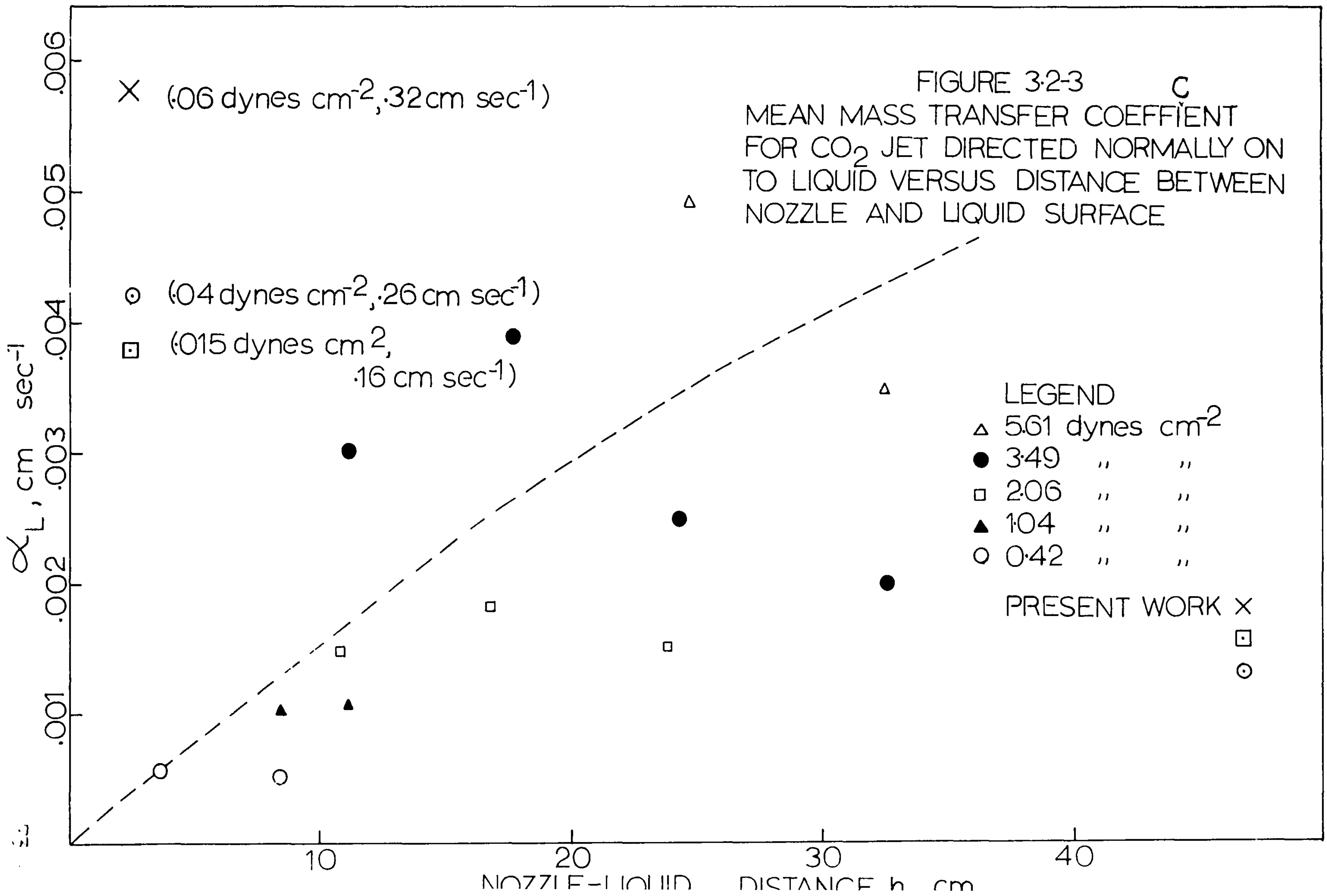

FIGURE 3·2·3

MEAN MASS TRANSFER COEFFIENT FOR CO_2 JET DIRECTED NORMALLY ON TO LIQUID VERSUS DISTANCE BETWEEN NOZZLE AND LIQUID SURFACE

The present mass transfer coefficient results are higher by a factor of about 10 over those which would be predicted from Wakelin's experimental results. Two contributing factors are:

(a) In the case of the H_2/steel experiments the space above the metal was enclosed possibly permitting a larger amount of circulation in the gas phase.

(b) More importantly, the melt was induction heated and the melt surface was, therefore, inadvertantly stirred by induction current forces.

An estimate of the effect of induction stirring can be obtained from the zero argon flow rate experiments for which α_L (calculated on the basis of C_H^{sL} is zero) has a maximum value of 0.4×10^{-2} cm $\sec^{-1}$. Mass transfer coefficients calculated on a similar basis at $t = 0$ for the various argon flow rates are:

Argon Flow Rate	α_L, $t = o$, $C_H^{sL} = o$
25	$.9 \times 10^{-2}$
40	1.3×10^{-2}
50	1.6×10^{-2}
50	1.3×10^{-2}

The induction stirring can be expected, therefore, to contribute about 1/2 of the mass transfer at the lowest flow rate (25 cm^3 $\sec^{-1}$) and 1/3 or 1/4 at the higher flow rates.

E Depth of Depression

The depressions beneath the jets during the argon degassing were clearly visible and the depths could be readily estimated. The depth estimates were 0.1 cm ± 0.05 cm (25 cm^3 sec^{-1}); 0.2 cm ± 0.1 cm (40 cm^3 sec^{-1}); and 0.3 cm ± 0.1 (50 cm^3 sec^{-1}).

These data have been applied to the dimensionless plot $\frac{\dot{M}}{\rho_L g h_o^3}$ vs. n_o/h_o suggested by Banks and Chandrasekhara(28), (Figure 3.2-4).

The experimental data of Wakelin(27) and Collins and Lubanska(29) are also shown in the Figure 3.2-4.

The depressions in the present work are in general agreement with the earlier dimensionless correlations, thus confirming their applicability to liquid steel.

F Rate of Hydrogen Removal - No Argon Flow

The rate of hydrogen removal when no jet of argon is being played on the bath is shown in Figure 3.2-1. In this case the crucible was open to the atmosphere.

It is interesting to note that the rate of hydrogen removal with no argon jet is never under a quarter of the maximum rate of hydrogen removal, i.e., at 50 cm^3 of Ar per second. In the no jet experiment it became apparent, however, that between 4 and 5 ppm of hydrogen remained in the melt after 15 minutes of exposure.

FIGURE 3·2-4

DIMENSIONLESS CORRELATION OF DEPTH OF DEPRESSION ,JET MOMENTUM AND DISTANCE OF NOZZLE ABOVE LIQUID SURFACE

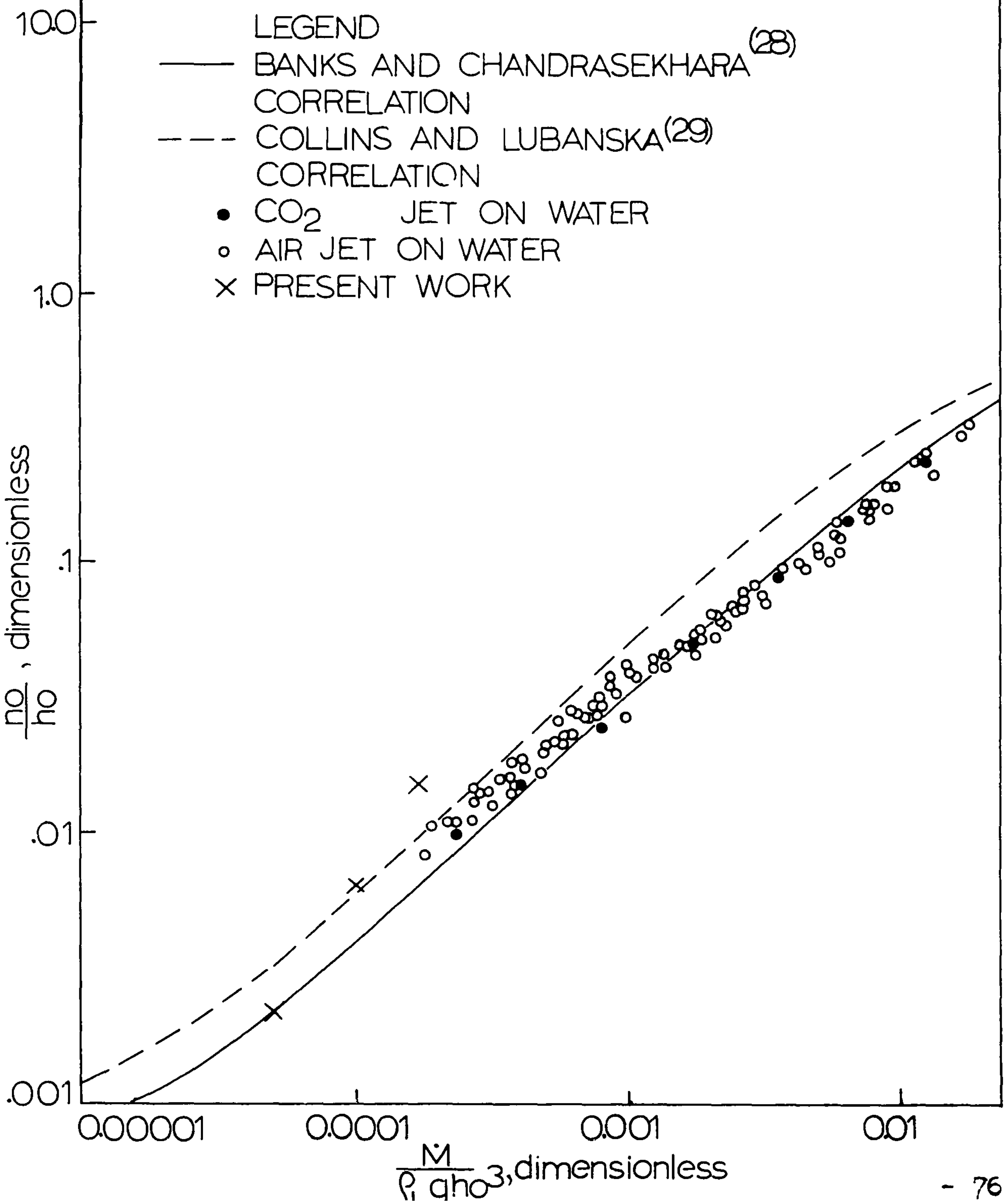

As previously mentioned, the rapid rate of hydrogen effusion is most likely due to turbulence created by the induction stirring.

The limited amount of hydrogen removal is due to the presence of water vapour in the atmosphere.

G Degassing Efficiency

Dewsnap and Hoyle(21) in their study of the efficiency of hydrogen removal showed that the minimum amount of argon required for degassing is

$$Ar_{273} = 0.131 \text{ PM} \left(\frac{1}{[H]_2} - \frac{1}{[H]_1} \right) \qquad \text{Eq. 3.2-10}$$

where Ar_{273} minimum volume of inert gas
(ft^3 at 273°K)

This expression assumes that the argon gas leaving the system is at equilibrium with the hydrogen in the metal.

Figure 3.2-5 shows a comparison of the Equation 3.2-10, Dewsnap and Hoyle(21) results, and the results of this work (basis - amount of argon to reduce hydrogen content to 1.78 ppm). The Dewsnap and Hoyle results are those for 75 lbs. of steel with a multiple lance of 20 holes placed 1-1/2 inches from the steel surface. Their argon flushing rate was 6.5 ft^3/min or in terms of characteristic velocity (NTP flow rate/bath area) 14 cm/sec.

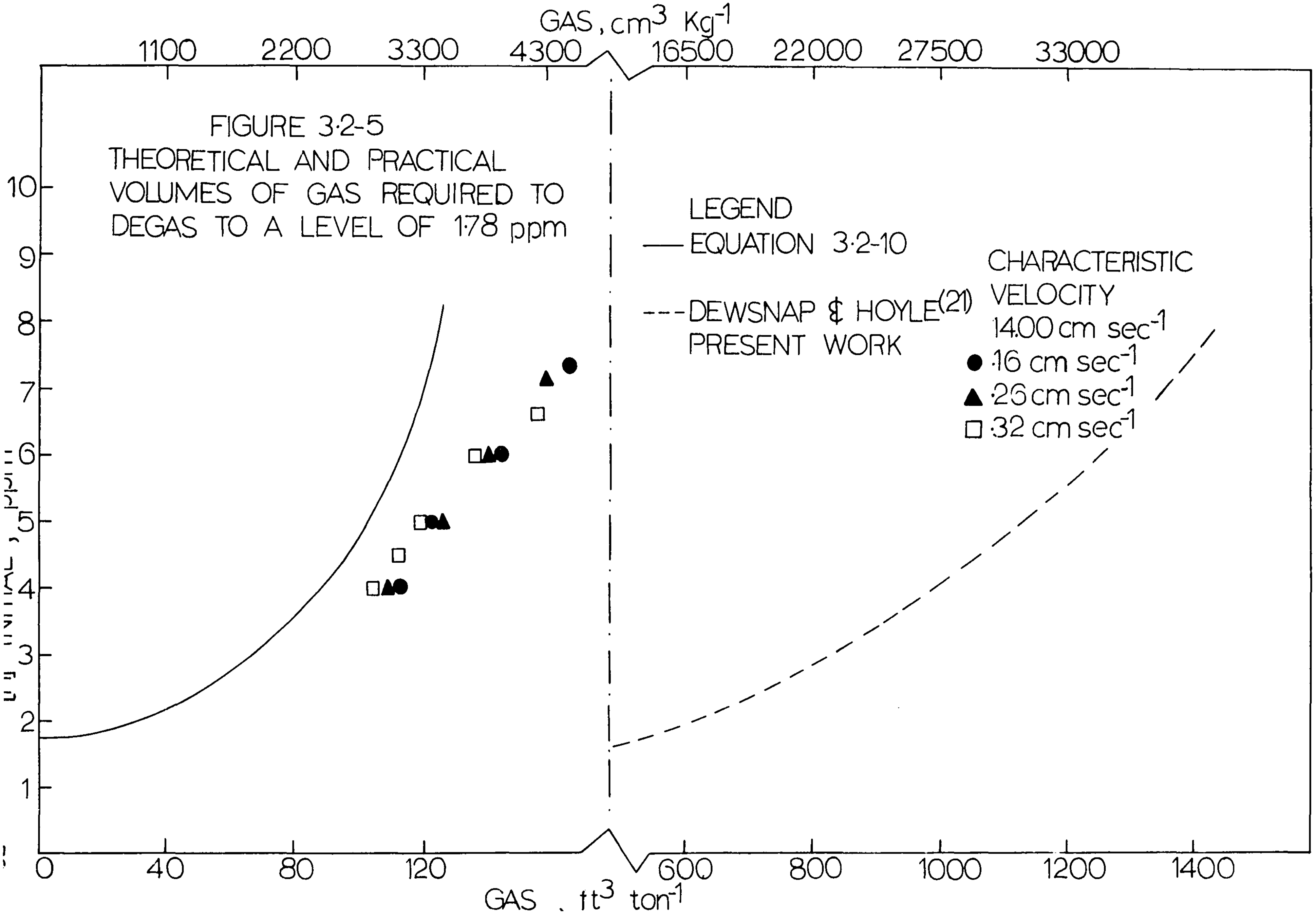

FIGURE 3·2-5
THEORETICAL AND PRACTICAL VOLUMES OF GAS REQUIRED TO DEGAS TO A LEVEL OF 1·78 ppm

Average efficiencies in the present work were:

Argon Flow Rate $cm^3\ sec^{-1}$	Characteristic Velocity $cm\ sec^{-1}$	Average Efficiency Percent
25	0.16	82
40	0.26	82
50	0.32	85

It is interesting to note that with the present arrangement, the efficiency of the argon gas is at least 70% of that predicted by Equation 3.2-10 (Figure 3.2-5). The Dewsnap and Hoyle(21) results, on the other hand, show that with high flow rate jets efficiencies of only 10% of theoretical are obtainable.

Earlier work of Hoyle(20) using a single lance 3 - 4 inches above the metal surface (lance inside diameter .2 cm) at a flow rate of 6 - 10 $ft^3\ min^{-1}$ (characteristic velocity 14 to 40 cm/sec) showed efficiencies similar to the Dewsnap and Hoyle results.

Argon flow rates in the Dewsnap and Hoyle work are some 60 to 100 times larger than the 50 $cm^3\ sec^{-1}$ of the present work but even at only 10% efficiency their hydrogen removal rates are some 6 - 10 times those found in the present work.

In an industrial process the time of treatment for hydrogen removal is restricted by the amount of superheat in the steel. It is clear, then, that low velocity jets alone cannot be used for hydrogen removal on an industrial scale. It may be possible, however, to combine argon bubble flushing for rapid hydrogen removal with low velocity argon jets to ensure a low final hydrogen content.

H Combined Bubbling and Flushing Process

The most important result of the present work is that even with a flow of 25 cm^3 of Ar per second, the hydrogen concentration was brought down to below 2 ppm.

It is of interest to determine the flow rates necessary to give equivalent treatment to ladles of steel having various top surface areas. A suitable criterion for equivalence is that the radial velocity at the crucible edge should be the same as that in the present tests.

If the jet is considered to be a point source and if the flow from this point source is planar, $U_r r$ will be constant with radius and proportional to the mass flow rate of the jet. The following flow rates would be required to be equivalent to 25 $cm^3\ sec^{-1}$ and the experimental 14 cm crucible diameter, i.e. for equivalent U_r at the outside radius of the crucible.

Radius	Argon Flow to Maintain U_r at Outside Radius
Exptal 7 cm	25 cm^3 sec^{-1}
1 foot (30 cm)	107 cm^3 sec^{-1}
2 feet (60 cm)	214 cm^3 sec^{-1}
3 feet (90 cm)	321 cm^3 sec^{-1}

The amount of argon required to reduce the hydrogen content by bubbling and to simultaneously protect the melt surface with a low velocity jet can be calculated from these data and from previous inert gas bubbling work.

The following conditions, which are similar to the Houston and Death(19) experimental argon bubbling conditions, have been chosen for the calculations:

Weight of steel:	2,000 lbs.
Hydrogen elimination:	10 ppm to 2 ppm
Radius of Melt Surface: (depth 17 inches)	12 inches
Time of exposure:	10 minutes

The amount of Argon (273°K, 1 atmospheres of argon pressure) theoretically required to reduce the hydrogen content from 10 to 2 ppm can be calculated using Equation 3.2-10 from which $Ar_{273°K} = 105\ ft^3\ (2.97 \times 10^6\ cm^3)$. If the argon is 60% efficient as reported by Houston and Death(19) the amount of gas required will be in the order of $5 \times 10^6\ cm^3$.

Over the same time period (10 minutes) the amount of argon introduced via jet to ensure a final 2 ppmH level will be (from the velocity-radius correlation on page 81 for a 1 foot radius) 600 seconds x 107 cm^3 sec^{-1} $\cong$ 6 x 10^4 cm^3, i.e., equivalent to an increase of approximately 1% in total argon flow.

The relative amount of gas introduced via the jet will vary with the shape of the vessel (surface area/depth ratio) and with the rate of bubbled gas introduction, but the gas jetted onto the surface will only be in the order of a few percent of the bubbled gas.

Until industrial test results become available there is no guarantee that a bubbling process accompanied by a jet surface protection would be successful in producing steel of less than 2 ppm hydrogen. If the present results are valid for large scale degassing tests, however, low flow rate jetting may find some industrial importance.

4.0 CONCLUSIONS

Studies of bubbles rising in thin sheets of mercury and thin sheets of water indicate that the dynamic behaviour of bubbles is similar in aqueous and liquid metal systems.

Rising velocities in thin sheets of liquid are larger than predicted by Collins most likely due to a partially three dimensional character of flow around the bubble, i.e., down one face of the bubble. At small volumes the rising velocities approach the three dimensional predictions of Davies and Taylor.

The angles subtended by the cylindrical surfaces in thin sheets of liquid are 60° - 70° as compared with 45° - 60° observed in three dimensional systems. This result is consistent with theoretical analyses of two dimensional and three dimensional flow.

Studies of hydrogen removal from steel have shown that it is possible to reduce hydrogen contents below 2 ppm by means of low flow-rate jets.

Mass transfer coefficients based upon diffusion of hydrogen in steel as the rate controlling step are an order of magnitude larger than would be expected from earlier model studies at room temperature due in part to induction and convection stirring in the melt.

The tests showed that argon efficiencies in the order of 80% of theoretical can be obtained as compared with 60% for bubbling and 10% for high flow rate jets.

Calculations based upon argon bubbling for hydrogen removal and low flow rate argon jetting for surface protection have been made. The argon required for surface protection and a resultant low H concentration (2 ppm or less) is shown to be only a few percent of the argon injected as bubbles.

Industrial tests of argon bubbling plus surface protection with low velocity argon jets are required to prove the viability of the process.

APPENDIX

The gas inside the covered crucible may be considered as in the diagram.

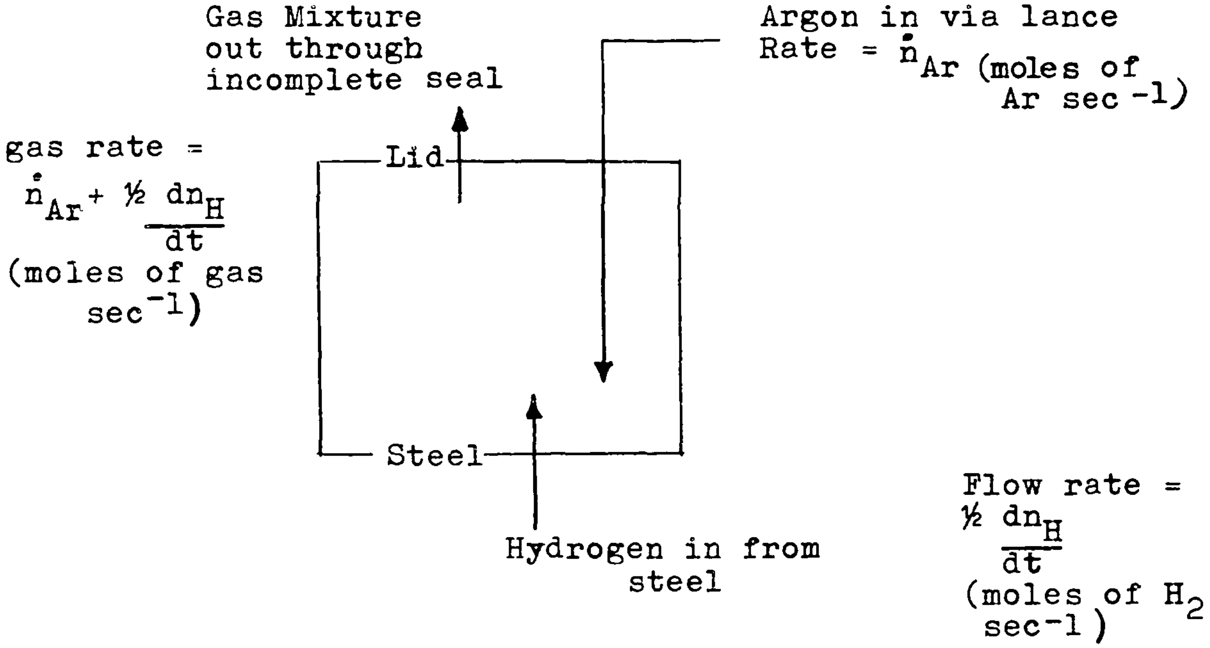

If the gas is completely and instantaneously mixed then the hydrogen concentration in the effluent gas is the same as in the enclosed space, i.e., $\frac{n_{H_2}}{n_{Ar} + n_{H_2}}$ (moles of H_2 per mole of gas)

which at 1 atmosphere total pressure is P_{H_2}.

From the equation of continuity:

Rate of H_2 in - Rate of H_2 out = Rate of Accumulation of H_2 in enclosed space.

or:

$$\frac{1}{2}\frac{dn_H}{dt} - \left\{\dot{n}_{Ar} + \frac{1}{2}\frac{dn_H}{dt}\right\} P_{H_2} = \frac{d\,P_{H_2}}{dt}\left(\frac{V}{RT}\right)$$

where V is the volume of the enclosed space.

If the rate of accumulation of H_2 in the enclosed space is small compared with the exit rate in the effluent gas then:

$$\frac{1}{2}\frac{dn_H}{dt} = \left\{ \dot{n}_{Ar} + \frac{1}{2}\frac{dn_H}{dt} \right\} P_{H_2}$$

and:

$$P_{H_2} = \frac{\frac{1}{2}\, dn_H}{\dot{n}_{Ar} + \frac{1}{2}\frac{dn_H}{dt}} \qquad \text{Eq. 3.2-7}$$

(Page 68)

Proof that rate of accumulation in the gas space is small compared with the total amount of hydrogen evolved is obtained by considering the present case of degassing 5 Kg of steel from 8 to 2 ppm.

Total hydrogen evolved in the gas is 1.5×10^{-2} moles. The maximum that P_{H_2} can change over this concentration range is the difference in equilibrium with 8 and 2 ppm, i.e., 0.08 atmospheres (Equation 3.2-5). With a 1000 cm^3 enclosed space, the maximum possible moles of hydrogen accumulated is 5×10^{-4} moles or only 3 percent of total quantity of hydrogen evolved.

NOTATION

A	Apparent area of bath surface	(cm^2)
Ar_{273}	Volume of inert gas at 273°K	(ft^3)
C^s_H	Saturation concentration of H at 1 atmos. H_2 pressure	(wt%)
C^{bL}_H	Overall bulk concentration of hydrogen in the steel bath	(g-atoms cm^{-3})
C^{sL}_H	Concentration of hydrogen in the steel bath at the metal surface	(g-atoms cm^{-3})
$C^{bL}_{CO_2}$	Concentration of carbon dioxide in the bulk liquid	(g-moles cm^{-3})
$C^{bg}_{CO_2}$	Concentration of carbon dioxide in the bulk gas	(g-moles cm^{-3})
D	Diffusion coefficient	(cm^2 sec^{-1})
d	Diameter of absorption tube (Equation 3.2-6)	(cm)
F	Henry's Law equilibrium coefficient C_{CO_2}/P_{CO_2}	(g-moles cm^{-3} $atmos^{-1}$)
g	Gravitational acceleration	(cm sec^{-2})
$[H]$	Hydrogen concentration	(ppm)
$[H]^b$	Bulk hydrogen concentration	(ppm)
$[H]^s$	Surface hydrogen concentration	(ppm)
h	Maximum vertical dimension of bubble	(cm)
h_o	Height of nozzle exit above liquid surface	(cm)
M	Weight of steel	(lbs.)
$\dot{M}$	Momentum of jet per unit time	(gr cm^{-1} sec^{-2})
n	Depth of surface depression below jet	(cm)
n_{CO_2}	Quantity of CO_2 in system	(g-moles)

n_H	Gram atoms of hydrogen in steel bath	(g-atoms)
$\dot{n}_{Ar}$	Argon molar flow rate in jet	(moles sec^{-1})
n_i	G-moles of i in the system	(g-moles)
P	Total pressure on system	(atmos)
P_c	Pressure of bubble in the cup	(atmos)
P_t	Pressure of bubble at the upper surface of mercury	(atmos)
$P^{sg}_{H_2}$	Pressure of hydrogen in the gas at the gas metal interface	(atmos)
$P^{bg}_{H_2}$	Pressure of hydrogen in the bulk gas	(atmos)
q	Velocity of fluid on bubble surface	(cm sec^{-1})
R_c	Radius of curvature (See Figure 2.3-1)	(cm)
R	Gas constant	(cm^3 atmos °K^{-1} g-moles^{-1})
r	Radius of spherical bubble	(cm)
r_e	Equivalent radius (i) two dimensional system $\left(\frac{\text{area of bubble}}{\pi}\right)^{1/2}$ (ii) three dimensional system $\left(\frac{\text{area of bubble seen by camera}}{\pi}\right)^{1/2}$	(cm)
T	Absolute temperature	(°K)
t	Time	(sec)
U	Terminal rising velocity	(cm sec^{-1})
U_r	Radial velocity	(cm sec^{-1})

V_c	Bubble volume in the cup	(cm^3)
V_t	Bubble volume at the upper surface of mercury	(cm^3)
w	Maximum horizontal dimension of bubble	(cm)
Z	Depth below the liquid surface	(cm)
θ	Angle at a point on bubble surface (from the vertical)	(-)
α	Subtended angle described by bubble surface	(-)
ρ_m	Density of liquid metal	(g cm^{-3})
ρ_g	Density of gas	(g cm^{-3})
ρ_r	Density of liquid	(g cm^{-3})
μ	Viscosity	(g cm^{-1} sec^{-1})
α_L	Mass transfer coefficient (liquid phase control)	(cm sec^{-1})
α_g	Mass transfer coefficient (gas phase control)	(cm sec^{-1})
α_o	Overall mass transfer coefficient (liquid and gas phase control)	(cm sec^{-1})

ACKNOWLEDGEMENTS

Sincere appreciation is extended to Professor W.G. Davenport who supervised this work.

Thanks are due to Professor W.M. Williams, Head, Department of Metallurgical Engineering, McGill University, for his encouragement and for making available the facilities of the Department.

The author wishes to extend his thanks to Mr. M. Knoepfel for his technical assistance.

The author is indebted to the National Research Council for providing financial assistance.

REFERENCES

1. Biggero, G., Elementi di Metallografia, Siderea, 1964 Rome, Page 11.
2. Parson, D.E., and Morgan, W.A., Can. Min. and Met. Bull, 1961, Vol. 54, page 163-169.
3. Peebles, F.N., and Garber, H.J., Chem. Eng. Prog., 1953, Vol. 49, page 88-97.
4. Garner, F.H., and Hammerton, D., Chem. Eng. Sci., 1954, Vol. 3, page 1-11.
5. Haberman, W.L., and Morton, R.K., Trans. Amer. Soc. of Civil Engineers, 1956, Vol. 121, page 227-250.
6. Hartunian, R.A., and Sears, W.R., J. Fluid Mech., 1957, Vol. 3, page 27-47.
7. Davenport, W.G., Bradshaw, A.V., and Richardson, F.D., J. Iron and Steel Inst., 1967, Vol. 205, page 1034-1042.
8. Guthrie, R.I.L., PH.D. Thesis, University of London, 1967.
9. Davenport, W.G., Richardson, F.D., and Bradshaw, A.V., Chem. Eng. Sci., 1967, Vol. 22, page 1221-1235.
10. Uno, S., and Kintner, R.C., J. Amer. Inst. Chem. Eng., 1956, Vol. 2, page 420-425.
11. Davies, R.M., and Taylor, G.I., Proc. Roy. Soc., 1950, Vol. A200, page 375-390.
12. Rippin, P.W.T., and Davidson, J.F., Chem. Eng. Sci., 1967, Vol. 92, page 217-228.
13. Collins, R., J. Fluid Mech., 1965, Vol. 22, page 763-771.
14. Baird, M.H.I., and Davidson, J.F., Chem. Eng. Sci., 1962, Vol. 17, page 87-93.

15. Collins, R., Chem. Eng. Sci., 1967, Vol. 22, page 88-97.

16. Walters, J.K., and Davidson, J.F., J. Fluid Mech., 1962, Vol. 12, page 408-416.

17. Grace, J.R., and Harrison, D., Chem. Eng. Sci., 1967, Vol. 22, page 1337-1347.

18. Vergé, J., Duflot, J., Spire, E., and Michaud, M., Revue de Met., 1961, Vol. 58, page 465-482.

19. Houston, R., and Death, F.S., J. of Met., 1967, Vol. 15, page 205-209.

20. Hoyle, G., J. Iron and Steel Inst., 1962, Vol. 200, page 605-610.

21. Dewsnap, P. and Hoyle, G., J. Iron and Steel Inst., 1965, Vol. 203, page 988-994.

22. Higbie, R., Trans. Amer. Inst. Chem. Eng., 1935, Vol. 31, page 365.

23. Dankwerts, P.V., Ind. Eng. Chem., 1951, Vol. 43, page 1460-1466.

24. Whitman, W.G., Chem. and Met. Eng., 1923, Vol. 29, page 146.

25. El-Tayeb, N.M., and Parlee, N.A.D., Trans. A.I.M.E., 1967, Vol. 239, page 1345-1351.

26. Chemical Engineers' Handbook, 4th Edition, McGraw Hill, New York, 1963, page 1419-1420.

27. Davenport, W.G., Wakelin, D.H., and Bradshaw, A.V., Heat and Mass Transfer in Process Metallurgy, Inst. of Mining and Metallurgy, 1967, London, page 207-244.

28. Banks, R.P., and Chandrasekhara, D.V., J. Fluid Mech., 1963, Vol. 15, page 13-14.

29. Collins, R.D., and Lubanska, H., Brit. J. App. Phys., 1954, Vol. 5, page 22-26.